International Journal of Heat and Mass Transfer 66 (2013) 338–348

Contents lists available at ScienceDirect

International Journal of Heat and Mass Transfer

journal homepage: www.elsevier.com/locate/ijhmt

Application of the lattice Boltzmann method combined with large-eddy simulations to turbulent convective heat transfer

Shing-Cheng Chang, Yue-Tzu Yang, Cha'o-Kuang Chen *, Wei-Lin Chen

Department of Mechanical Engineering, National Cheng Kung University, Tainan, Taiwan

ARTICLE INFO

Article history:
Received 28 December 2012
Received in revised form 24 June 2013
Accepted 27 June 2013

Keywords:
Lattice Boltzmann method
Large-eddy simulation
Turbulence
Heat transfer

ABSTRACT

In this paper, the large-eddy simulation is introduced into the lattice Boltzmann method to study convective heat transfer in turbulent flows. The simulations include a closed lid-driven cavity flow and a backward-facing step flow in both laminar and turbulent regions. The results show that by combining with large-eddy simulations, the lattice Boltzmann method can simulate turbulent flow phenomena well and give good agreement with other experimental and numerical results, while the traditional lattice Boltzmann method fails. Quaternary vortices of the turbulent cavity flows are captured in the simulations as well as the transient vortices of backward-facing step flows. By calculating the distribution of skin-friction coefficients and Nusselt number on the lower wall, the drag and heat transfer efficiency of backward-facing step flows are found to be influenced by the vortices generated near walls significantly, no matter the flow is laminar or turbulent. For laminar cases, the flow phenomena are also greatly affected by the Reynolds number. But in turbulence, the flow field is fully perturbed and chaotic, so that the transport phenomena are approximately independent of the Reynolds number.

1. Introduction

The lattice Boltzmann method (LBM) [1,2] has been developed over twenty years and achieved considerable success in many problems. On the basis of the microscopic nature, the LBM simulates fluid flows by performing a bottom-up scheme, which treats the fluid particles on a statistical level. Simplified kinetic models incorporating essential physics of microscopic processes are constructed in the LBM. Fluid flows are tracked through the evolution of one-particle phase space distribution functions and associated macroscopic averaged properties. Based on the gas kinetic theorem, LBM simulations include two steps, namely particle distribution "collisions" on lattice nodes and stream "propagations" from one node to all neighbors along the lattice directions. After streaming, new distribution components on lattice nodes are obtained from neighbors in a new time step and cause new local and macroscopic properties. Essentially, this is different from other traditional CFD methods, which analyze flow fields by solving macroscopic variables in the Navier–Stokes equations.

As a promising method of computational fluid dynamics (CFD), many difficult problems in traditional CFD can be solved by LBM, e.g. multiphase fluid flows [3], heat transfer [4], microfluidics [5], fluid flows through porous media [6] and fractal geometry [7]. In nature and engineering, turbulent flows are very common. But they are difficult to be solved by theoretical or numerical schemes because of the complicated and irregular characteristics. Therefore, to simulate turbulent flows by the LBM is an attractive topic [8]. Chen and Doolen [9] summarized the lattice Boltzmann method for fluid flows, which included the development of LBM for simulating turbulence. The typical methods for simulating turbulence are direct numerical simulation (DNS), Reynolds average numerical simulation (RANS), and large-eddy simulation (LES), which was proposed first by Deardoff [10]. The base ideal of LES is to decompose the turbulent flow field into large and small scale parts. The large scale part is solved by Navier–Stokes equations, while the small scale part is solved by sub-grid scale (SGS) model.

The SGS model used in this study is based on the well-known Smagorinsky model [11], which includes vortex-viscous and vortex-diffusive forms. Hou et al. [12] used LBM coupled with the standard Smagorinsky model and introduced the eddy relaxation time to simulate two-dimensional driven cavity flow. The Reynolds number was considered up to 100,000. Chen [13] also used a large-eddy-based LBM to simulate turbulent driven cavity flow. This model is corresponding to vorticity-stream function equations and hence has better numerical stability than the traditional LBM, which solves mass density, pressure and velocity for Navier–Stokes equations. Guan and Wu [14] introduced two sub-grid models, namely the dynamics SGS model and the dynamical system SGS model, to the lattice Boltzmann method for solving

* Corresponding author. Tel.: +886 6 2757575x62140.
E-mail address: ckchen@mail.ncku.edu.tw (C.-K. Chen).

0017-9310/$ - see front matter © 2013 Elsevier Ltd. All rights reserved.
http://dx.doi.org/10.1016/j.ijheatmasstransfer.2013.06.067

three dimensional high Re turbulent driven cavity flows. Results were compared with those obtained from the Smagorinsky model and direct numerical simulation for the same cases.

Although the large-eddy simulation was proposed and applying to study turbulence for decades, the combination of the lattice Boltzmann method and LES were extensively adopted only in recent years. To our knowledge, there are a few studies concerning solving convection heat transfer in turbulence, and most of these studies were focused on the topic of a closed cavity [15–20]. Wu et al. [21] simulated the turbulent heat transfer in a channel flow. Although their work included three dimensional effects, the channel walls were two straight plates. The objective of this study is to apply the LBM by combining with the LES to simulate turbulence. The simulations include the lid-driven cavity flow and the backward-facing step flow. In addition, the turbulent heat transfer phenomena in the backward-facing step flow are simulated and discussed.

For the backward-facing step flow, the separation and reattachment phenomena produce the recirculation region downstream the step. Armaly et al. [22] used the laser-Doppler measurements to observe velocity distribution and reattachment length of a single backward-facing step in a channel. The numerical method was also applied to simulate this problem. The discussions were presented for laminar, transitional and turbulent flow of air in a Reynolds number range of $70 < Re < 8{,}000$. The results indicated that the flow can be considered as laminar for $Re < 1{,}200$ and turbulent for $Re > 6{,}600$. For the range of $1{,}200 < Re < 6{,}600$, the flow phenomena are transitional and present noticeable three dimensional effects. Since the present simulations are considered two dimensional cases, this work focuses on the laminar and turbulent regions of the backward-facing step flow only. The reattachment length for the laminar region is also compared with numerical results of Erturk [23] and Ma et al. [24]. For the turbulent region, Jongebloed's numerical results [25] by FULENT with RANS method for turbulence are adopted for validation. Otherwise, the drag effects and heat transfer efficiency are evaluated by calculating the skin-friction coefficients and the Nusselt number, respectively. Finally, the turbulent convective heat transfer phenomena of the backward-facing step flow are discussed in this paper.

2. Numerical methods

2.1. Hydrodynamic model for LBM

The Boltzmann equation with a linearized collision operator can be written as follows:

$$\frac{\partial f}{\partial t} + \vec{v}\cdot\frac{\partial f}{\partial \vec{x}} = \frac{1}{\tau_f}(f^{eq} - f), \tag{1}$$

where $\vec{v}$ is microscopic velocity. The relaxation term on the right side is the simplified collision operator, namely the Bhatnagar–Gross–Krook (BGK) approximation model [26], with the relaxation time τ_f for the density distribution function f towards the local equilibrium. The equilibrium distribution function f^{eq} is related to the Maxwell–Boltzmann equilibrium distribution. By applying a lattice model of a discrete velocity set, the Boltzmann equation with BGK model (LBGK) can be transformed into the discrete form of

$$\frac{\partial f_\alpha}{\partial t} + \vec{e}_\alpha\cdot\nabla f_\alpha = -\frac{1}{\tau_f}(f_\alpha - f_\alpha^{eq}), \tag{2}$$

where $f_\alpha(\vec{x},t)$ and $\vec{e}_\alpha$ are the component of density distribution function and lattice velocity vector in the α direction of the lattice model. For evolution of distribution function, this discrete lattice Boltzmann equation can be discretized in the time and space domain as

$$f_\alpha(\vec{x}+\vec{e}_\alpha\Delta t, t+\Delta t) - f_\alpha(\vec{x},t) = -\frac{1}{\tau_f}[f_\alpha(\vec{x},t) - f_\alpha^{eq}(\vec{x},t)]. \tag{3}$$

The LBGK model can be decomposed as two steps repeated for each time step, namely stream and collision steps. These steps are performed individually in different lattice directions according to the specified lattice model.

In the LBM simulation, the DnQb lattice model proposed by Qian et al. [27] of n dimension and b lattice velocities are often used. This study adopts the convenient D2Q9 lattice model [4,7] for both the hydrodynamic and thermal analysis of flows. The discrete velocity set of D2Q9 model is shown in Fig. 1. The velocity distribution are defined as

$$\vec{e}_\alpha = \begin{cases} (0,0) & ,\alpha = 0 \\ c\left[\cos((\alpha-1)\frac{\pi}{2}), \sin\left((\alpha-1)\frac{\pi}{2}\right)\right] & ,\alpha = 1\text{–}4 \\ \sqrt{2}c\left[\cos\left((2\alpha-1)\frac{\pi}{4}\right), \sin\left((2\alpha-1)\frac{\pi}{4}\right)\right] & ,\alpha = 5\text{–}8 \end{cases} \tag{4}$$

where $c = \Delta x/\Delta t = \Delta y/\Delta t$ is the lattice streaming speed defined by time step Δt and the grid spacing Δx and Δy. The density equilibrium distribution function is given by

$$f_\alpha^{eq} = \rho\omega_\alpha\left[1 + \frac{\vec{e}_\alpha\cdot\vec{u}}{c_s^2} + \frac{(\vec{e}_\alpha\cdot\vec{u})^2}{2c_s^4} - \frac{u^2}{2c_s^2}\right], \tag{5}$$

where $\omega_\alpha = \frac{4}{9}$ for $\alpha = 0$, $\omega_\alpha = \frac{1}{9}$ for $\alpha = 1$–4, and $\omega_\alpha = \frac{1}{36}$ for $\alpha = 5$–8. $\vec{u}(\vec{x},t)$ is the velocity vector at the lattice node of position $\vec{x}$. The macroscopic density and velocity are calculated as

$$\rho = \sum_\alpha f_\alpha, \tag{6}$$

$$\vec{u} = \frac{1}{\rho}\sum_\alpha f_\alpha\vec{e}_\alpha. \tag{7}$$

By the Chapman–Enskog expansion [2], the LBGK model can be recovered to the macroscopic equations as follows

$$\frac{\partial\rho}{\partial t} + \nabla\cdot(\rho\vec{u}) = 0, \tag{8}$$

$$\frac{\partial}{\partial t}(\rho\vec{u}) + \nabla\cdot(\rho\vec{u}\vec{u}) = -\nabla p + \nabla\cdot\left\{\rho\nu\left[\nabla\vec{u} + (\nabla\vec{u})^T\right] - \frac{\nu}{c_s^2}\nabla\cdot(\rho\vec{u}\vec{u}\vec{u})\right\}, \tag{9}$$

where $p = \rho c_s^2$ is the pressure related to the lattice sound speed, $c_s = c/\sqrt{3}$. The kinematic viscosity is

$$\nu = c_s^2\left(\tau_f - \frac{1}{2}\right)\Delta t. \tag{10}$$

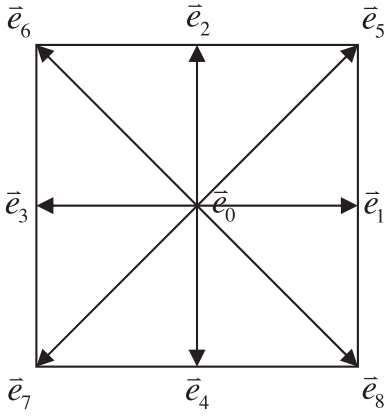

Fig. 1. D2Q9 model for LBM simulation.

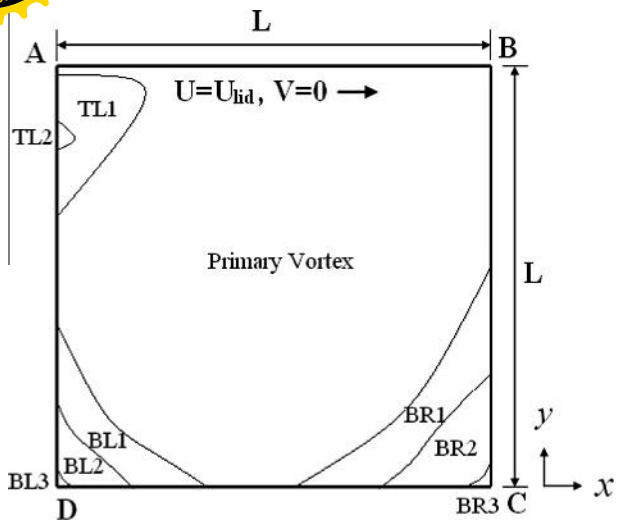

Fig. 2. Schematic view of lid-driven cavity flows.

Eq. (8) is continuity equation, and Eq. (9) has a deviation term $\frac{v}{c_s^2}\nabla\cdot(\rho\vec{u}\vec{u}\vec{u})$ compared with Navier–Stokes equations. With the low Mach number assumption, $Ma = u/c_s \ll 1$, this deviation term can be neglected. For the incompressible flow, the LBGK model gives the continuity equation and Navier–Stokes equations as

$$\nabla\cdot\vec{u} = 0, \tag{11}$$

$$\frac{\partial\vec{u}}{\partial t} + \nabla\cdot(\vec{u}\vec{u}) = -\frac{1}{\rho}\nabla p + \nu\nabla^2\vec{u}. \tag{12}$$

2.2. Thermal model for LBM

The present study adopts the thermal model by Shan [28], which is based on the model proposed by Shan and Chen [29] for simulating flows with multi-phases and -components. This model simulates the flows with heat transfer by density distribution function as described above and temperature distribution function. The evolution equation of temperature distribution function is expressed as

$$g_\alpha(\vec{x}+\vec{e}_\alpha\Delta t, t+\Delta t) - g_\alpha(\vec{x},t) = -\frac{1}{\tau_g}\left[g_\alpha(\vec{x},t) - g_\alpha^{eq}(\vec{x},t)\right], \tag{13}$$

where τ_g is the relaxation time of the temperature distribution function $g_\alpha(\vec{x},t)$. The temperature equilibrium distribution function for the D2Q9 lattice model is given by

$$g_\alpha^{eq} = T\omega_\alpha\left[1 + \frac{\vec{e}_\alpha\cdot\vec{u}}{c_s^2} + \frac{(\vec{e}_\alpha\cdot\vec{u})^2}{2c_s^4} - \frac{u^2}{2c_s^2}\right], \tag{14}$$

where $\omega_\alpha = \frac{4}{9}$ for $\alpha = 0$, $\omega_\alpha = \frac{1}{9}$ for $\alpha = 1$–4, and $\omega_\alpha = \frac{1}{36}$ for $\alpha = 5$–8. $T(\vec{x},t)$ is the temperature at the lattice node of position $\vec{x}$ The macroscopic temperature is then calculated as

$$T = \sum_\alpha g_\alpha. \tag{15}$$

The macroscopic energy equation without viscous heat dissipation and compression work can be derived from the Eq. (13) for the temperature distribution function by Chapman–Enskog expansion [28] as

$$\frac{\partial T}{\partial t} + \nabla\cdot(T\vec{u}) = \kappa\nabla^2 T, \tag{16}$$

where the diffusivity κ is determined by

$$\kappa = c_s^2\left(\tau_g - \frac{1}{2}\right)\Delta t. \tag{17}$$

2.3. The LBM combined with large-eddy simulation

In large-eddy simulation [10], the physical quantities are decomposed into large and small scale parts by the filtering process. The filter process as follows

$$\bar{\Phi} = \frac{1}{\Delta^3}\int_{-\Delta/2}^{\Delta/2}\int_{-\Delta/2}^{\Delta/2}\int_{-\Delta/2}^{\Delta/2}\Phi(\bar{\xi},t)G(\bar{x}-\bar{\xi})d\xi_1 d\xi_2 d\xi_3, \tag{18}$$

where Φ represents the physical quantity before filter process, e.g. density, velocity, pressure, temperature, and etc., while $\bar{\Phi}$ is the large scale physical quantity after filter process. Δ is the filter length equal to the mesh length. The spatial filter function, G, used in this paper is the box filter function as follows,

$$G(\vec{x}-\vec{\xi}) = \begin{cases} 1 & ,|\vec{x}-\vec{\xi}| \le \frac{\Delta}{2}, \\ 0 & ,|\vec{x}-\vec{\xi}| > \frac{\Delta}{2}. \end{cases} \tag{19}$$

By filtering the density and temperature distribution function, the hydrodynamic and thermal LBM models with large-eddy simulations can be obtained with the same forms as before filtering [12].

Table 1
Locations of the vortex center in lid-driven cavity flows at $1000 \leqq Re \leqq 7500$ (steady flows). The symbol "-" denotes no vortices appeared in this position.

Vortex position	Scheme	Location, (x, y)			
		Re = 1000	Re = 2500	Re = 5000	Re = 7500
Primary vortex	LBM	(0.5320, 0.5660)	(0.5202, 0.5439)	(0.5133, 0.5331)	(0.5113, 0.5297)
	LBM-LES	(0.5319, 0.5656)	(0.5200, 0.5440)	(0.5130, 0.5334)	(0.5108, 0.5302)
	Erturk et al. (2005)	(0.5300, 0.5650)	(0.5200, 0.5433)	(0.5150, 0.5350)	(0.5133, 0.5317)
BR1	LBM	(0.8647, 0.1141)	(0.8357, 0.0940)	(0.8032, 0.0759)	(0.7886, 0.0679)
	LBM-LES	(0.8646, 0.1142)	(0.8354, 0.0940)	(0.8021, 0.0760)	(0.7868, 0.0681)
	Erturk et al. (2005)	(0.8633, 0.1117)	(0.8350, 0.0917)	(0.8050, 0.0733)	(0.7900, 0.0650)
BL1	LBM	(0.0837, 0.0774)	(0.0865, 0.1104)	(0.0758, 0.1349)	(0.0675, 0.1505)
	LBM-LES	(0.0837, 0.0774)	(0.0865, 0.1104)	(0.0756, 0.1347)	(0.0674, 0.1501)
	Erturk et al. (2005)	(0.0833, 0.0783)	(0.0850, 0.1100)	(0.0733, 0.1367)	(0.0650, 0.1517)
TL1	LBM	–	(0.0421, 0.8850)	(0.0637, 0.9020)	(0.0678, 0.9060)
	LBM-LES	–	(0.0418, 0.8847)	(0.0633, 0.9017)	(0.0668, 0.9052)
	Erturk et al. (2005)	–	(0.0433, 0.8900)	(0.0633, 0.9100)	(0.0667, 0.9133)
BR2	LBM	(0.9919, 0.0081)	(0.9906, 0.0092)	(0.9768, 0.0177)	(0.9528, 0.0364)
	LBM-LES	(0.9919, 0.0081)	(0.9906, 0.0092)	(0.9763, 0.0180)	(0.9516, 0.0375)
	Erturk et al. (2005)	(0.9917, 0.0067)	(0.9900, 0.0100)	(0.9783, 0.0183)	(0.9517, 0.0417)
BL2	LBM	–	–	–	(0.0105, 0.0107)
	LBM-LES	–	–	–	(0.0105, 0.0107)
	Erturk et al. (2005)	(0.0050, 0.0050)	(0.0067, 0.0067)	(0.0083, 0.0083)	(0.0117, 0.0117)

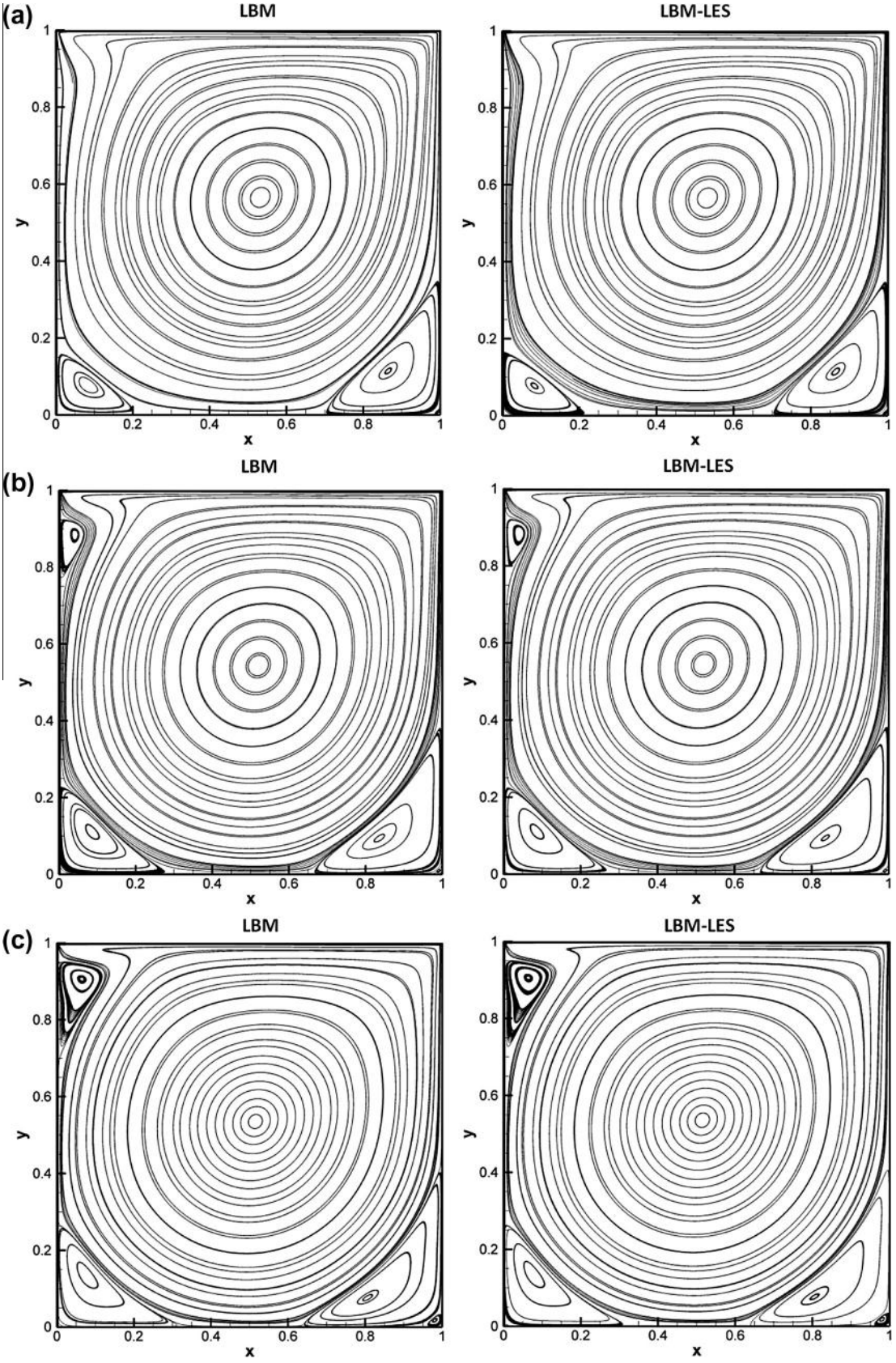

Fig. 3. Streamlines of lid-driven cavity flows at Re = (a) 1000, (b) 2500, (c) 5000, (d) 7500 and (e) 10,000 by the LBM and LBM-LES simulation. The last case is unsteady and changed into turbulence, while others are laminar.

In this LBM-LES model, the viscosity and diffusivity, ν and κ, are replaced by the equivalent quantities, $\nu_{total} = \nu + \nu_t$ and $\kappa_{total} = \kappa + \kappa_t$, in which ν_t and κ_t are eddy viscosity and eddy diffusivity respectively. For specific Reynolds number, $\mathrm{Re} = UL/\nu$, and Prandtl

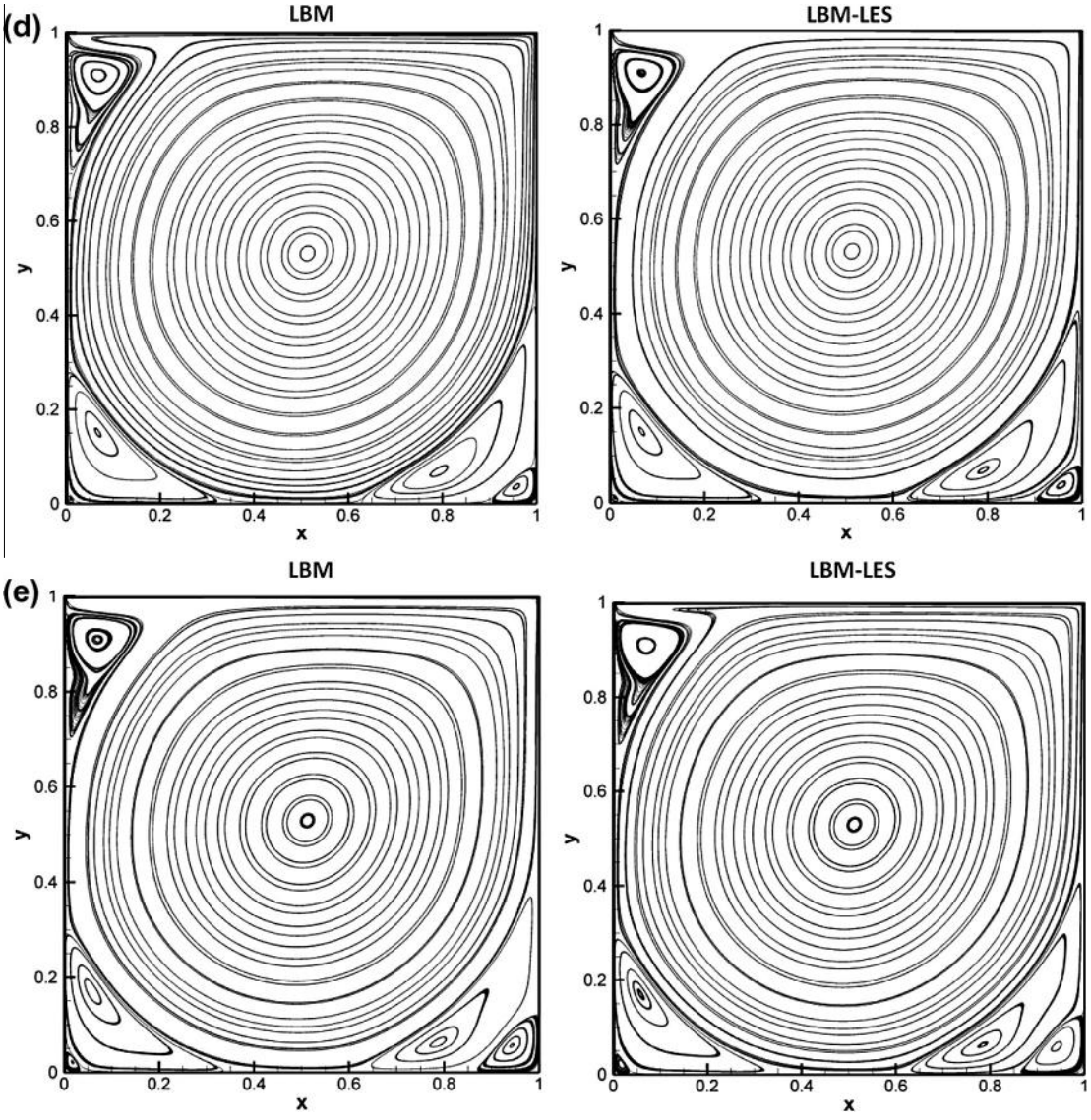

Fig. 3 (*continued*)

Number, $\mathrm{Pr} = \nu/\kappa$, of the flow, ν and κ are specified. In the Smagorinsky model, eddy viscosity is represented as

$$\nu_t = (C_s\Delta)^2|\bar{S}|, \tag{20}$$

where $C_s > 0$ is the Smagorinsky constant. In this paper, the Smagorinsky constant is fixed as $C_s = 0.1$. $|\bar{S}|$ is the magnitude of strain rate tensor given by

$$|\bar{S}| = \frac{\sqrt{\tau_f^2 + \frac{18\sqrt{2}(C_s\Delta)^2 Q^{\frac{1}{2}}}{\rho}} - \tau_f}{6(C_s\Delta)^2}, \tag{21}$$

where Q is the magnitude of the non-equilibrium stress tensor, Π_{ij}, and calculated as

$$Q = \Pi_{ij}\Pi_{ij}, \tag{22}$$

$$\Pi_{ij} = \sum_{\alpha} e_{\alpha i} e_{\alpha j}\left(f_\alpha - f_\alpha^{eq}\right). \tag{23}$$

As the molecular diffusivity κ, the eddy diffusivity κ_t can be obtained by defining the sub-grid Prandtl Number as

$$\mathrm{Pr}_t = \frac{\nu_t}{\kappa_t}. \tag{24}$$

According to Eqs. (10) and (19), the equivalent relaxation time $\tau_{f|total}$ and $\tau_{g|total}$ for LBM-LES equations are obtained.

2.4. Implements of boundary conditions and convergence criteria

In the time evolution of distribution function, there exist certain unknowns on boundary nodes because no distributions are propagated from wall nodes into the flow. By applying appropriate method, these unknowns can be solved for specific boundary conditions. In this study, the no-slip boundary condition of the stationary wall is realized by the common bounce-back rule [30], which assumes the unknowns are the same as the distribution functions in the opposite direction. The boundary condition of a given velocity or temperature is implemented by the forced-equilibrium method [12]. This scheme gives boundary unknowns to be equal to the local equilibrium distribution functions as

$$f_\alpha(\vec{x}_b, t+\Delta t) = f_\alpha^{eq}(\vec{x}_b, t), \tag{25}$$

$$g_\alpha(\vec{x}_b, t+\Delta t) = g_\alpha^{eq}(\vec{x}_b, t), \tag{26}$$

where $\vec{x}_b$represents the position at the boundary node. For the velocity boundary condition of the inlet, the forced-equilibrium

Table 2
Locations of the vortex center in lid-driven cavity flows at 10,000 ≦ Re ≦ 20,000 (unsteady flows). The symbol "-" denotes no vortices appeared in this position.

Vortex position	Scheme	Location (x, y)			
		Re = 10000	Re = 15000	Re = 17500	Re = 20000
Primary vortex	LBM	(0.5122, 0.5296)	Divergence	Divergence	Divergence
	LBM-LES	(0.5115, 0.5304)	(0.5101, 0.5287)	(0.5100, 0.5282)	(0.5096, 0.5285)
	Erturk et al. (2005)	(0.5117, 0.5300)	(0.5100, 0.5283)	(0.5100, 0.5267)	(0.5100, 0.5267)
BR1	LBM	(0.7831, 0.0629)	Divergence	Divergence	Divergence
	LBM-LES	(0.7776 , 0.0625)	(0.7135, 0.0403)	(0.7241, 0.0443)	(0.7372, 0.0494)
	Erturk et al. (2005)	(0.7767, 0.0600)	(0.7483, 0.0500)	(0.7367, 0.0467)	(0.7267, 0.0450)
BL1	LBM	(0.0594, 0.1683)	Divergence	Divergence	Divergence
	LBM-LES	(0.0558, 0.1759)	(0.0511, 0.1923)	(0.0532, 0.1908)	(0.0556, 0.1855)
	Erturk et al. (2005)	(0.0583, 0.1633)	(0.0533, 0.1717)	(0.0517, 0.1750)	(0.0483, 0.1817)
TL1	LBM	(0.0700, 0.9101)	Divergence	Divergence	Divergence
	LBM-LES	(0.0696, 0.9101)	(0.0732, 0.9087)	(0.0721, 0.9082)	(0.0717, 0.9081)
	Erturk et al. (2005)	(0.0717, 0.9117)	(0.0767, 0.9117)	(0.0800, 0.9133)	(0.0817, 0.9133)
BR2	LBM	(0.9406, 0.0586)	Divergence	Divergence	Divergence
	LBM-LES	(0.9382, 0.0614)	(0.9239, 0.0865)	(0.9281, 0.1053)	(0.9293, 0.1015)
	Erturk et al. (2005)	(0.9350, 0.0667)	(0.9267, 0.0883)	(0.9283, 0.0967)	(0.9300, 0.1033)
BL2	LBM	(0.0170, 0.0200)	Divergence	Divergence	Divergence
	LBM-LES	(0.0190, 0.0258)	(0.0570, 0.0549)	(0.0785, 0.0547)	(0.0842, 0.0534)
	Erturk et al. (2005)	(0.0167, 0.0200)	(0.0367, 0.0417)	(0.0483, 0.0483)	(0.0567, 0.0533)
TL2	LBM	–	Divergence	Divergence	Divergence
	LBM-LES	–	(0.0200, 0.8297)	(0.0214, 0.8296)	(0.0218, 0.8291)
	Erturk et al. (2005)	–	(0.0150, 0.8267)	(0.0200, 0.8233)	(0.0233, 0.8200)
BR3	LBM	–	Divergence	Divergence	Divergence
	LBM-LES	–	–	(0.9909, 0.0088)	(0.9841, 0.0187)
	Erturk et al. (2005)	(0.9967, 0.0050)	(0.9950, 0.0050)	(0.9950, 0.0067)	(0.9933, 0.0067)
BL3	LBM	–	Divergence	Divergence	Divergence
	LBM-LES	–	–	–	(0.0169, 0.0092)
	Erturk et al. (2005)	(0.0017, 0.0017)	(0.0017, 0.0033)	(0.0033, 0.0033)	(0.0033, 0.0033)

method is found to have a higher numerical stability in turbulent channel flows than other schemes, e.g. the common method for velocity and pressure boundary conditions by Zou and He [31].

The present work simulates both laminar and turbulent flows in the lid-driven cavity and the backward-facing step by using the LBM-LES model. For laminar regions, the following inequalities are used as the criteria of convergence:

$$\frac{\sum_{i,j}|\vec{V}(\vec{x}_{i,j},t+\Delta t)-\vec{V}(\vec{x}_{i,j},t)|}{\sum_{i,j}|\vec{V}(\vec{x}_{i,j},t)|}\leqslant 1.0\times 10^{-7}, \tag{27}$$

$$\frac{\sum_{i,j}|T(\vec{x}_{i,j},t+\Delta t)-T(\vec{x}_{i,j},t)|}{\sum_{i,j}|T(\vec{x}_{i,j},t)|}\leqslant 1.0\times 10^{-7}. \tag{28}$$

In order to capture the unsteady flow phenomena in turbulence, the time average of turbulent physical quantity is evaluated and calculated as

$$\langle\Phi(\vec{x})\rangle=\frac{\sum_{t=T_s}^{T_E}\Phi(\vec{x},t)}{T_E-T_s} \tag{29}$$

where $\langle\rangle$ means computing the time average of the duration from time step T_s to T_E, in which the flow is reached the numerical stability.

3. Results and discussion

In the LBM-LES simulation, all equations and physical quantity are non-dimensionalized by the lattice length, Δx, lattice speed, c, and reference density, ρ_0. The dimensionless temperature is defined as $T^*=(T-T_{in})/(T_w-T_{in})$. The numerical simulation is confirmed to be grid independent.

3.1. The lid-driven cavity flow

Fig. 2 shows the schematic view of the cavity flow with a driving lid from left to right. In this case, a primary vortex is found typically in the center of the cavity accompanied with secondary vortices appeared at bottom right (BR), bottom left (BR), and top left (TL) corners. The number following these abbreviations refers to the vortices according to size. Since the D2Q9 model is subjected to a low Mach number, the velocity of the lid (A–B) is fixed to $U_{lid}=0.1c$. Hence the Reynolds number is changed by different dimensionless kinematic viscosity. The other stationary walls adopt no-slip boundary conditions.

This study adopts both the LBM and LBM-LES to simulate lid-driven cavity flow, and compares the results with Erturk et al. [32]. Table 1 shows the results of 1,000 ≦ Re ≦ 7,500, in which the flow phenomena are laminar and steady. The streamlines by these two methods are identical as shown in Fig. 3. At low Re = 1,000, only a primary vortex near the center and a pair of secondary ones in the lower corners of the cavity are apparent. The vortex in the upper left corner is produced as Re increased to 2,500. In the cases of Re = 5,000 and 7,500, it is found that the tertiary vortex in the lower right corner is enlarged. The tertiary one in the lower left corner is also formed gradually in these cases. The data in Table 1 also present that the primary vortex and the secondary ones in the lower corners move toward the center of the cavity as Re increases.

The simulation results show that the flow is laminar and steady in the cases of Re ≦ 7,500 and changed into turbulence when Re ≧ 10,000. These unsteady phenomena are captured by calculating time average of the physical quantity in the simulation, as shown in Table 2. It is noticed that the LBM simulation without a turbulence model would be numerical divergence in the cases of Re ≧ 15,000, while the LBM-LES simulation gives analogous results as Erturk et al. [32] at Re up to 20,000. The results in Table 2 and Fig. 4(a) show the tertiary vortex in the lower left corner is enlarged accompanied with another one appeared in the upper left corner at Re = 15,000. For flows in higher Re, the quaternary vortices can be found in lower right and left corners. The present results give good agreement with Erturk et al. [32] and show that by combining with the LES turbulence model, the applicability of the LBM simulation can be extended from laminar flow to turbulence.

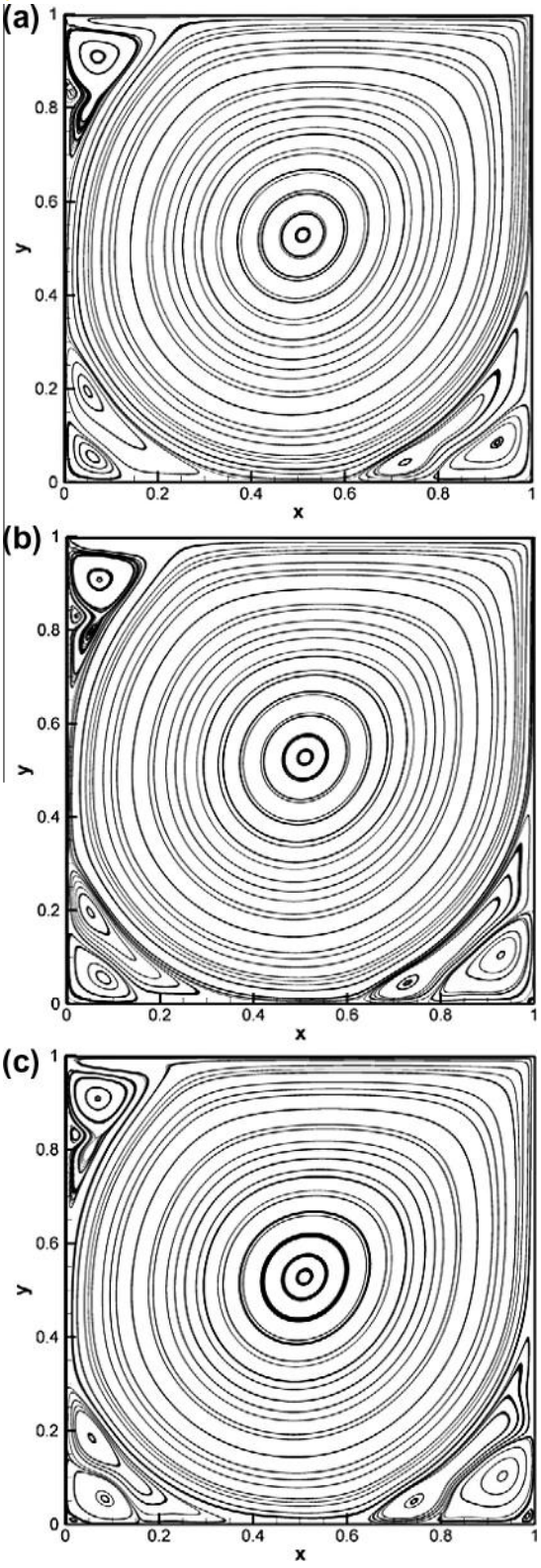

Fig. 4. Streamlines of turbulent lid-driven cavity flows at Re = (a) 15,000, (b) 17,500 and (c) 20,000 by the LBM-LES simulation.

3.2. The backward-facing step flow

In this section, the laminar and turbulent phenomena of backward-facing step flow are investigated by the LBM and LBM-LES simulation and compared with other experimental and numerical results. Moreover, the convective heat transfer in the channel is also discussed. Fig. 5 is the schematic view of the backward-facing step flow with expansion ratio $ER = H/h = 2$. The inlet and outlet length are 40 h and 100 h respectively. The Reynolds number is defined as

$$\mathrm{Re} = \frac{U_{in}H}{\nu}, \tag{30}$$

where U_{in} is the average velocity of the fully developed flow at inlet (A–F) and fixed to $0.1c$ for a low Mach number. The Prandtl number and subgrid Prandtl Number is fixed as 1.0 and 0.7. The temperature of inlet flow is constant as $T = T_{in}$. The stationary walls adopt no-slip boundary conditions and a high constant temperature $T = T_w > T_{in}$. At the outlet boundary (B and C), the flow is assumed to be fully developed, i.e. $\partial U/\partial x = \partial V/\partial x = \partial T/\partial x = 0$, and the pressure is fixed.

Fig. 6 shows the streamlines of the backward-facing step flow at $\mathrm{Re} \leqq 1{,}000$. The flow phenomena are laminar with a main recirculation region downstream the step. As Re increases, this region is enlarged due to the enhancing convective effect. Otherwise, a secondary recirculation region is also produced near the upper wall. Actually, several recirculation regions will be generated near both upper and lower walls if Re is high enough. To investigate the characteristic of a backward-facing step flow, the detachment and reattachment length of the recirculation region is often used [23]. In this work, only the reattachment length of main recirculation region, $x1/S$, is discussed. The results shown in Fig. 7 are close to the numerical results by Erturk [23] and Ma et al. [24] and have the similar tendency as the experiment results by Armaly et al. [22].

Armaly et al. [22] indicated the backward-facing flow is laminar at Re < 1,200 and turbulent at Re > 6,600. In the laminar region, the velocity in the flow field is steady. Fig. 8(a) shows the fluid velocity observed at the location of (S, S) downstream the step is tended to convergence after 50,000 run time steps. But when the flow is changed into turbulence, the fluid velocity is unsteady, i.e. the velocity of turbulence is perturbed with time but gives a stable time average, as shown in Fig. 8(b). In the turbulent backward-facing step flow, more small transient vortices behind the step are formed. Fig. 9 shows the streamlines at $6{,}600 \leqq \mathrm{Re} \leqq 9{,}000$, in which the reattachment lengths of main recirculation region are smaller than those of laminar flows at $\mathrm{Re} \geqq 600$. Armaly et al. [22] indicated the reattachment length almost kept constant as $x1/S = 8$ at $\mathrm{Re} \geqq 6{,}600$. Jongebloed's work [25] presented similar results by using FLUENT but a shorter reattachment length than Armaly et al. [22]. The comparison is listed in Table 3 with the present results. The secondary vortex near upper wall in Fig. 9 is also presented a smaller size than that of laminar flow.

For the laminar region, the LBM simulation gives the same results as the LBM-LES simulation. But in turbulent region, the LBM simulation will present numerical divergence. The results above show that the LBM-LES model presents feasibility for simulating laminar and turbulent phenomena in a channel flow as well as in a closed lid-driven cavity flow. Since the LBM-LES simulation presents good accuracy with other experimental or numerical results, this paper extends the scheme to the thermal analysis to study the convective heat transfer phenomena in the laminar and turbulent flow of the backward-facing step. The temperature distribution is shown in Figs. 10 and 11. In this case, the cold fluid from inlet is heating by the hot walls via the heat transfer between walls and fluid, and hence the fluid temperature is increased downstream. In laminar cases, an intermediate region of cold fluid is formed by the effects of heat conduction and convection. As Re increases, the convective effect is enhanced so that the intermediate cold region can be extended downstream further. However, thermal diffusivity is still dominant near the wall boundary and in the region of recirculation, in which the convection is restrained. Since the flow

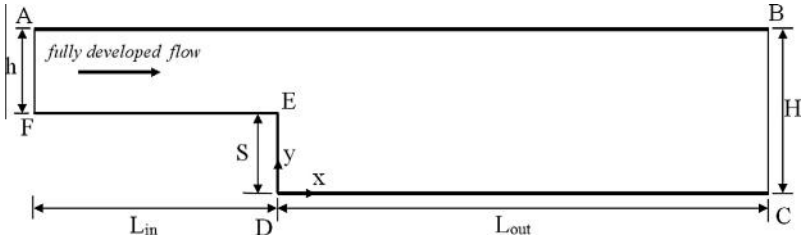

Fig. 5. Schematic view of the backward-facing step flows.

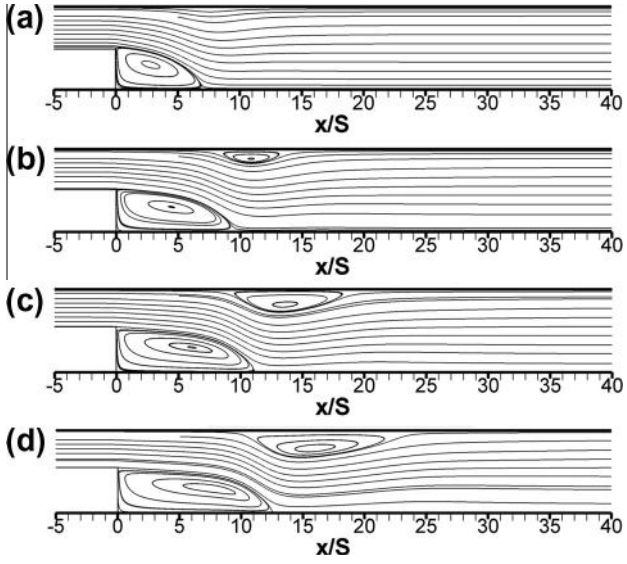

Fig. 6. Streamlines of laminar backward-facing step flows at Re = (a) 400, (b) 600, (c) 800 and (d) 1000.

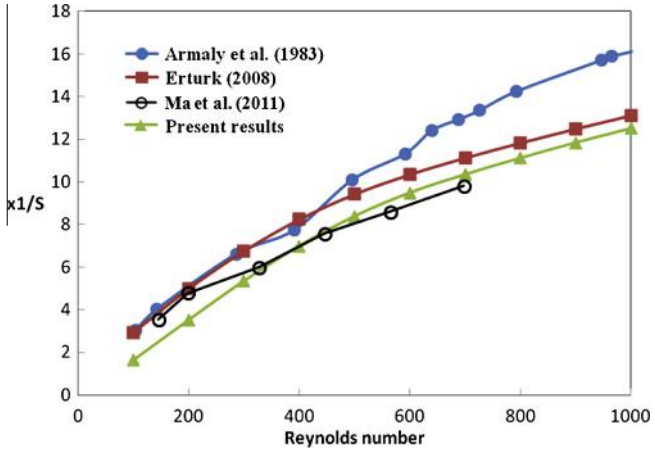

Fig. 7. The reattachment length of laminar backward-facing step flows. ($100 \leqq Re \leqq 1000$).

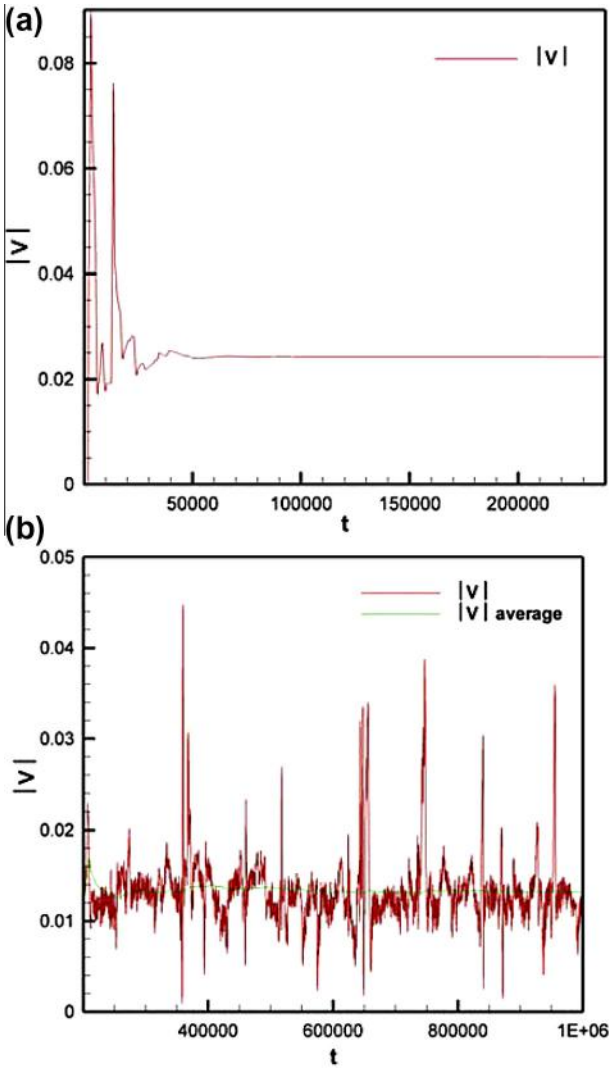

Fig. 8. Temporal velocities at location (S, S). (a) Laminar flow at Re = 1000; (b) turbulence at Re = 6600.

field is strongly perturbed in turbulence, there are no intermediate regions found downstream, i.e. the downstream temperature distribution of fluid is uniform. The difference of temperature contours at $6600 \leqq Re \leqq 9000$ is unapparent, as shown in Fig. 11. It presents that the convective effect is dominant everywhere, including wall boundaries and recirculation regions. Therefore, the fluid heating, or namely the wall cooling, is very fast and efficient.

To further estimate the magnitude of drag and the heat transfer effect of the backward-facing step flow, the skin-friction coefficient [33], ReC_f, and the Nusselt number, Nu, on the lower wall boundary D and C downstream the step are calculated. The skin-friction coefficient, C_f, is defined as

$$C_f = \frac{\tau_w}{\rho U_{in}^2}, \tag{31}$$

where the shear stress, τ_w, on the surface is

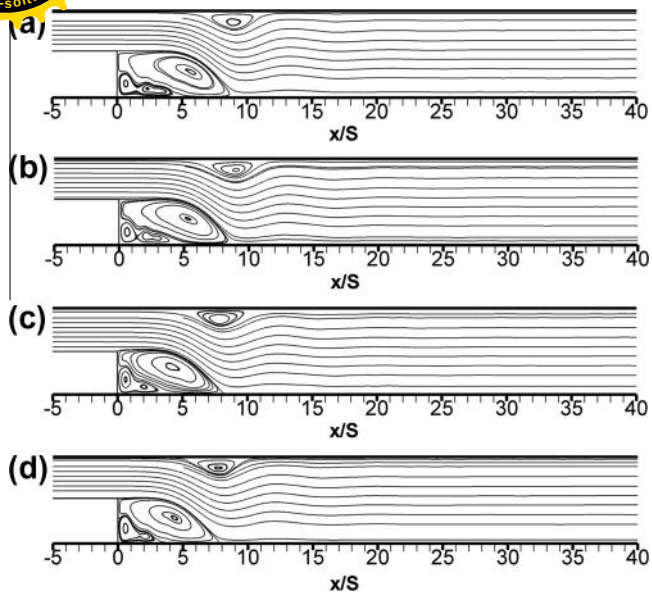

Fig. 9. Streamlines of turbulent backward-facing step flows at Re = (a) 6600, (b) 7000, (c) 8000 and (d) 9000.

Table 3
The reattachment length of turbulent backward-facing step flow.

Re	X1/S		
	Armaly et al. (1983)	Jongebloed (2008)	Present results
6600	8.05909	–	8.84
7000	8.01919	6.92	8.68
8000	8.0211	6.80	8.1
9000	–	–	7.8

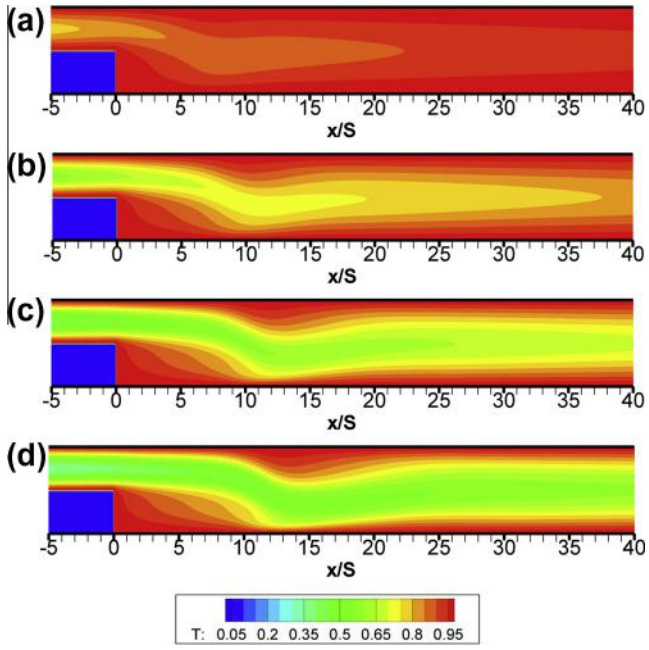

Fig. 10. Temperature distribution of laminar backward-facing step flows at Re = (a) 400, (b) 600, (c) 800 and (d) 1000.

$$\tau_w = \mu\left(\frac{\partial u}{\partial y} + \frac{\partial v}{\partial x}\right)_{y=S(x)}. \tag{32}$$

Substitution of Eq. (32) into Eq. (31) yields

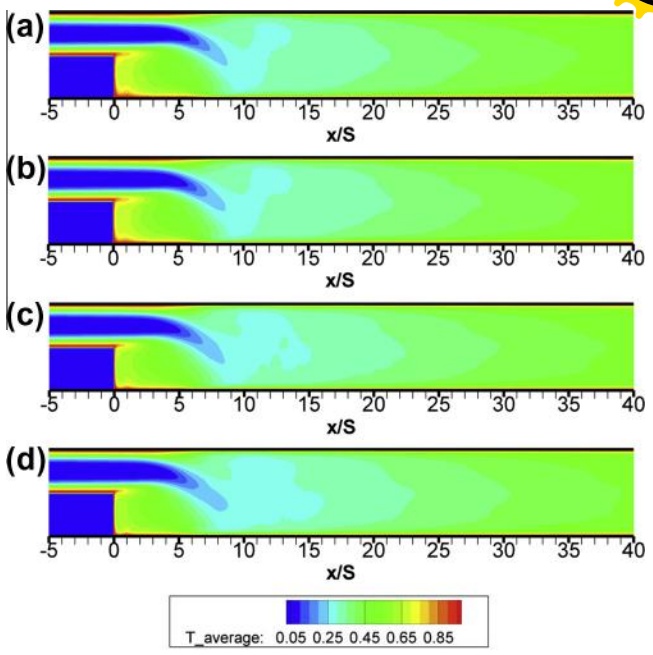

Fig. 11. Temperature distribution of turbulent backward-facing step flows at Re = (a) 6600, (b) 7000, (c) 8000 and (d) 9000.

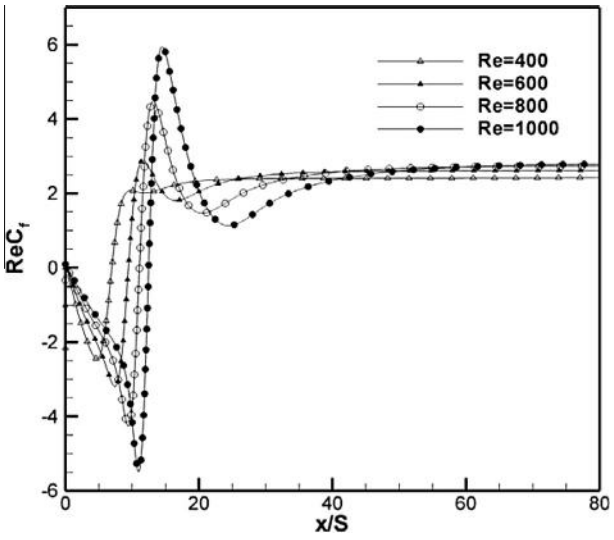

Fig. 12. Distribution of skin-friction coefficient for laminar backward-facing step flows at different Reynolds number.

$$\mathrm{Re}C_f = \frac{H}{U_{in}}\left(\frac{\partial u}{\partial y} + \frac{\partial v}{\partial x}\right)_{y=S(x)}. \tag{33}$$

The local Nusselt number at the surface is defined as

$$Nu_x = \frac{h_x H}{K_f} = \frac{-\left(\frac{\partial T}{\partial y}\right)H}{T_w - T_{in}}, \tag{34}$$

where h_x and K_f are heat transfer coefficient and thermal conductivity respectively.

Fig. 12 is the distribution of skin-friction coefficient for different Reynolds number in laminar backward-facing step flow. Since the flow reversal occurs behind the step, the skin-friction coefficient is negative in this region and changed to positive after the reattach-

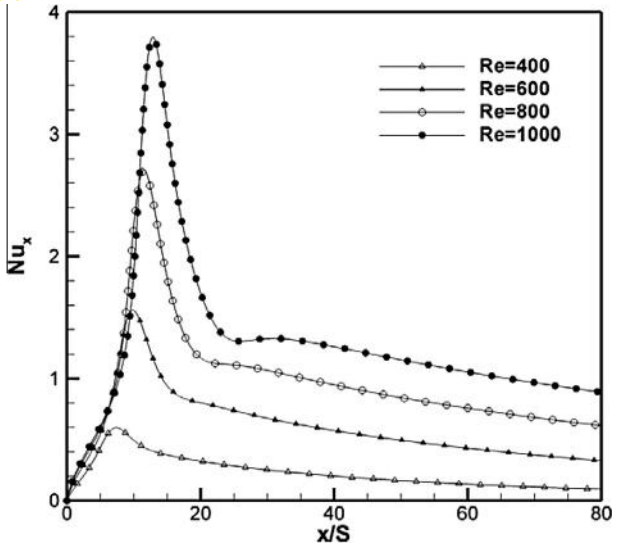

Fig. 13. Distribution of Nusselt number for laminar backward-facing step flows at different Reynolds number.

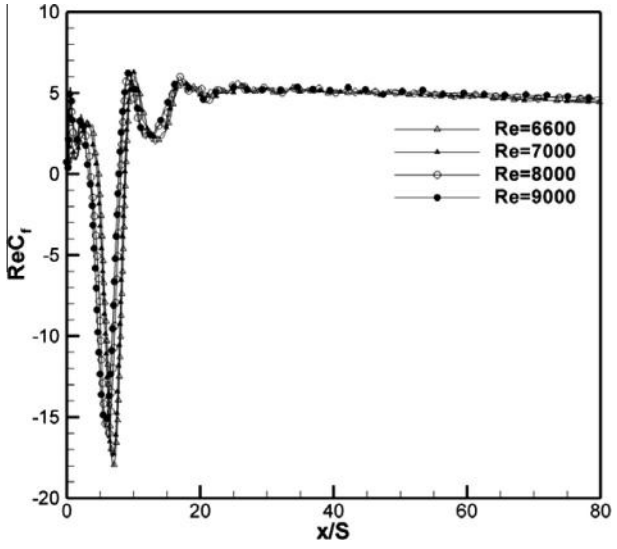

Fig. 14. Distribution of skin-friction coefficient for turbulent backward-facing step flows at different Reynolds number.

ment point. The minimum skin-friction coefficient occurs nearby the reattachment point which gives a large shear stress upon the surface. Subsequently, the positive skin-friction coefficient is increased downstream the reattachment point and reaches a constant value as a fully developed flow at outlet. For the cases high Re, the secondary vortex produced in the upper wall causes oppression of the fluid flow, and hence induces high stress on the bottom wall. Fig. 12 shows that the ReC_f curve would reach a peak at the location with greatest coverage of the upper secondary vortex. The effect of vortices nearby walls on the convective heat transfer is also significant. The Nusselt number in the case of Re = 400 shown in Fig. 13 reaches a maximum value at the main reattachment point and subsequently decays to a stable value of the outlet smoothly. The similar phenomena are occurred in the cases of high Re except for a sharp decreasing of Nu caused by the upper vortex.

For the laminar flow, increasing Re naturally enhances the convective heat transfer, and simultaneously causes the shear stress

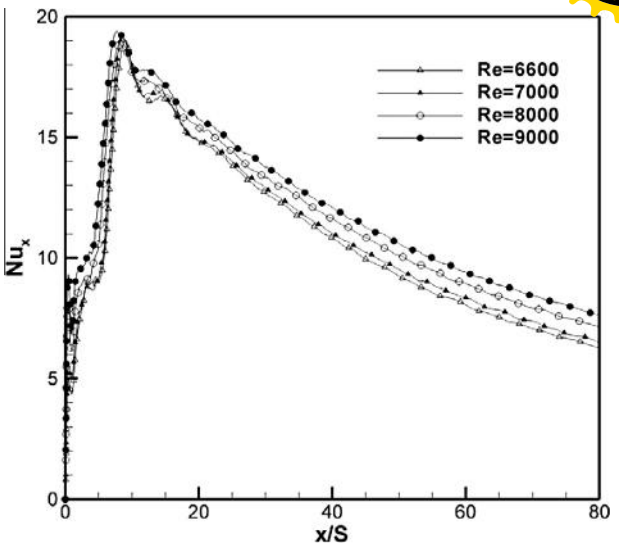

Fig. 15. Distribution of Nusselt number for turbulent backward-facing step flows at different Reynolds number.

raising. But for the turbulence, the increase of Re cannot give a great influence on the hydrodynamic and thermal properties of fluid flows. This is because that the flow field is chaotic as mentioned above. As the reattachment length of main recirculation region, the skin-friction coefficient and Nusselt number of the turbulent backward-facing step flow present small difference at different Reynolds number, as shown in Figs. 14 and 15. Nevertheless, for the backward-facing step flow, the Nusselt number in turbulence is much larger than in laminar flow, as well as the inducing stress on the walls.

4. Conclusion

In this paper, the lattice Boltzmann method combined with the large-eddy simulation is applied to simulate turbulent flow and hear transfer phenomena. First, a closed system of the lid-driven cavity flow is studied by both the LBM and LBM-LES simulation. In the laminar region, LBM simulation gives good agreement with other works as well as the LBM-LES model. The locations of vortices produced at bottom right, bottom left, and top left corners are captured in sequence correctly. As the flow changes into turbulence, LBM simulation without a turbulence model would be numerical divergence, whereas the LBM-LES scheme is still applicable. The unsteady phenomena of turbulence are investigated by evaluating time average of the physical quantity.

Subsequently, the backward-facing step flow is taken into account. As for the lid-driven cavity flow, the LBM simulation fails in the turbulent region, while the LBM-LES can simulate the unsteady turbulent phenomena well. For laminar flow, the reattachment length of main recirculation region behind the step is raised as Re increases, and so as the magnitude of drag force on the walls. Otherwise, the distribution of skin-friction coefficient shows that a large shear stress is imposed on the bottom surface nearby the primary reattachment point. The oppressive effect of the upper secondary vortex on the fluid also induces a high stress on the bottom wall. When the flow is far away the vortices, skin-friction coefficient would reach a constant value of the fully developed flow. In the turbulent region, the flow field is perturbed and chaotic with several small transient vortices generated backward the step. The main reattachment length shows independence of Re and keeps a value about $x1/S \approx 8$. A little difference of the skin-friction coefficient at different Re is also obtained in the simulation.

For the backward-facing step flow, the LES scheme is extended to the thermal LBM simulation to study the heat transfer phenomena. The effect of vortices on the heat convection is still significant and dominative. Especially in the turbulence, violent variation of the fluid flow causes a fast and efficient heat mixing. As for the skin-friction coefficient, the Nusselt number of the bottom wall raises as Re increases in the laminar region, but shows independence of Re for turbulence. The present work shows that by combining the LBM with LES simulation, the hydrodynamic and thermal analysis of a laminar flow or turbulence can be achieved. The results for both cavity and channel flow systems give good agreement with the work by other experimental or numerical methods.

Acknowledgements

This study acknowledges the support provided to this research by the National Science Council of Republic of China under Grant No. NSC 99-2221-E-006 -098 -MY2.

Appendix A. Supplementary data

Supplementary data associated with this article can be found, in the online version, at http://dx.doi.org/10.1016/j.ijheatmasstransfer. 2013.06.067.

References

[1] G.R. McNamara, G. Zanetti, Use of the Boltzmann equation to simulate lattice-gas automata, Phys. Rev. Lett. 61 (1988) 2332–2335.
[2] D.W. Gladrow, Lattice-Gas Cellular Automata and Lattice Boltzmann Models: An Introduction, Springer, 2000.
[3] D. Grunau, S. Chen, K. Eggert, A lattice Boltzmann model for multiphase fluid flows, Phys. Fluids 5 (1993) 2557–2562.
[4] C.K. Chen, S.C. Chang, S.Y. Sun, Lattice Boltzmann method simulation of channel flow with square pillars inside by the field synergy principle, CMES-Comput. Model. Eng. Sci. 22 (2007) 203–215.
[5] J. Zhang, Lattice Boltzmann method for microfluidics: models and applications, Microfluid. Nanofluid. 10 (2011) 1–28.
[6] Z. Guo, T.S. Zhao, Lattice Boltzmann model for incompressible flows through porous media, Phys. Rev. E 66 (2002) 036304.
[7] S.C. Chang, Y.S. Hsu, C.L. Chen, Lattice Boltzmann simulation of fluid flows with fractal geometry: an unknown-index algorithm, J. Chin. Soc. Mech. Eng. 32 (2011) 523–531.
[8] H. Chen, S. Kandasamy, S. Orszag, R. Shock, S. Succi, V. Yakhot, Extended Boltzmann kinetic equation for turbulent flows, Science 301 (2003) 633–636.
[9] S. Chen, G.D. Doolen, Lattice Boltzmann model for fluid flows, Annu. Rev. Fluid Mech. 30 (1998) 329–364.
[10] J.W. Deardoff, The use of subgrid transport equations in a three-dimensional model of atmospheric turbulence, J. Fluids Eng. Trans. ASME 95 (1973) 429–438.
[11] J.S. Smagorinsky, General circulation experiments with the primitive equations- I. The basic experiment, Mon. Weather Rev. 91 (1963) 99–164.
[12] S. Hou, J. Sterling, S. Chen, G.D. Doolen, A lattice Boltzmann subgrid model for high Reynolds number flows, in: A.T. Lawniczak, R. Kapral (Eds.), Pattern Formation and Lattice Gas Automata. Fields Institute Communications, 1996, pp. 151–166.
[13] S. Chen, A large-eddy-based lattice Boltzmann model for turbulent flow simulation, Appl. Math. Comput. 215 (2009) 591–598.
[14] H. Guan, C. Wu, Large-eddy simulations of turbulent flows with lattice Boltzmann dynamics and dynamical system sub-grid models, Sci. China Ser. E Technol. Sci. 52 (2009) 670–679.
[15] C.V. Treeck, E. Rank, M. Krafczyk, Extension of a hybrid thermal LBE scheme for large-eddy simulations of turbulent convective flows, Comput. Fluids 35 (2006) 863–871.
[16] H. Liu, C. Zou, B. Shi, Z. Tian, L. Zhang, C. Zheng, Thermal lattice-BGK model based on large-eddy simulation of turbulent natural convection due to internal heat generation, Int. J. Heat Mass Transfer 49 (2006) 4672–4680.
[17] S. Chen, M. Krafczyk, Entropy generation in turbulent natural convection due to internal heat generation, Int. J. Therm. Sci. 48 (2009) 1978–1987.
[18] S. Chen, J. Tölke, M. Krafczyk, Simple lattice Boltzmann subgrid-scale model for convectional flows with high Rayleigh numbers within an enclosed circular annular cavity, Phys. Rev. E 80 (2009) 026702.
[19] H. Sajjadi1, M. Gorji, G.H.R. Kefayati, D.D. Ganji, Lattice boltzmann simulation of turbulent natural convection in tall enclosures using cu/water nanofluid, Numer. Heat Transfer Part A 62 (2012) 512–530.
[20] S. Chen, H. Liu, C. Zheng, Numerical study of turbulent double-diffusive natural convection in a square cavity by LES-based lattice Boltzmann model, Int. J. Heat Mass Transfer 55 (2012) 4862–4870.
[21] H. Wu, J. Wang, Z. Tao, Passive heat transfer in a turbulent channel flow simulation using large eddy simulation based on the lattice Boltzmann method framework, Int. J. Heat Fluid Flow 32 (2011) 1111–1119.
[22] B.F. Armaly, F. Durst, J.C.F. Pereira, B. Schonung, Experimental and theoretical investigation of backward-facing step flow, J. Fluid Mech. 127 (1983) 473–496.
[23] E. Erturk, Numerical solutions of 2-D steady incompressible flow over a backward-facing step. Part I: high reynolds number solutions, Comput. Fluids 37 (2008) 633–655.
[24] K. Ma, W.L. Wei, L.L. Wang, X.J. Zhao, Large eddy numerical simulation of flows over a backward-facing step, Int. Symp. Water Res. Environ. Prot. 4 (2011) 3024–3026.
[25] L. Jongebloed, Numerical study using FLUENT of the separation and reattachment points for backwards-facing step flow, Master's thesis in mechanical engineering, Rensselaer Polytechnic Institute, 2008.
[26] P.L. Bhatnagar, E.P. Gross, M. Krook, A model for collision processes in gases. I. Small amplitude processes in charged and neutral one-component systems, Phys. Rev. 94 (1954) 511–521.
[27] Y.H. Qian, D. d'Humiéres, P. Lallemand, Lattice BGK models for Navier–Stokes equation, Europhys. Lett. 17 (1992) 479–484.
[28] X. Shan, Simulation of Rayleigh–Bénard convection using a lattice Boltzmann method, Phys. Rev. E 55 (1997) 2780–2788.
[29] X. Shan, H. Chen, Lattice Boltzmann model for simulating flows with multiple phases and components, Phys. Rev. E 47 (1993) 1815–1819.
[30] D.P. Ziegler, Boundary conditions for lattice Boltzmann simulation, J. Stat. Phys. 71 (1993) 1171–1177.
[31] Q. Zou, X. He, On pressure and velocity boundary conditions for the lattice Boltzmann BGK model, Phys. Fluids 9 (1997) 1591–1598.
[32] E. Erturk, T. Corke, C. Gokcol, Numerical solutions of 2-D steady incompressible driven cavity flow at high Reynolds numbers, Int. J. Numer. Methods Fluids 48 (2005) 747–774.
[33] C.C. Wang, C.K. Chen, Forced convection in a wavy-wall channel, Int. J. Heat Mass Transfer 45 (2002) 2587–2595.

World Academy of Science, Engineering and Technology
International Journal of Mechanical, Aerospace, Industrial and Mechatronics Engineering Vol:7 No:7, 2013

PDF-XChange Editor
Click to BUY NOW!
www.tracker-software.com

Lattice Boltzmann Method for Turbulent Heat Transfer in Wavy Channel Flows

H.Y. Lai, S. C. Chang, and W. L. Chen

***Abstract*—**The hydrodynamic and thermal lattice Boltzmann methods are applied to investigate the turbulent convective heat transfer in the wavy channel flows. In this study, the turbulent phenomena are modeling by large-eddy simulations with the Smagorinsky model. As a benchmark, the laminar and turbulent backward-facing step flows are simulated first. The results give good agreement with other numerical and experimental data. For wavy channel flows, the distribution of Nusselt number and the skin-friction coefficients are calculated to evaluate the heat transfer effect and the drag force. It indicates that the vortices at the trough would affect the magnitude of drag and weaken the heat convection effects on the wavy surface. In turbulent cases, if the amplitude of the wavy boundary is large enough, the secondary vortices would be generated at troughs and contribute to the heat convection. Finally, the effects of different Re on the turbulent transport phenomena are discussed.

***Keywords*—**Heat transfer, lattice Boltzmann method, turbulence, wavy channel.

I. Introduction

THE lattice Boltzmann equation (LBE) is developed from the lattice gas cellular automata (LGCA) by introducing ensemble-average density distribution function to substitute the Boolean operators in LGCA [1]. In the lattice Boltzmann method (LBM), the fluid flow is treated on a statistical level and calculated by a simplified kinetic model, in which macroscopic physical properties are associated with microscopic processes. This bottom-up scheme is different from traditional top-down schemes of computational fluid dynamics (CFD), which analyze flow fields by solving macroscopic variables in the Navier-Stokes equations. In recent years, the LBM has become a promising method of CFD, especially in mesoscopic engineering and science as microfluidics [2]. The LBM has been extensively applied to multiphase fluid flows [3], heat transfer [4], fluid flows through porous media [5], and etc. It possesses an advantage to implement boundaries with complex flow or fractal geometry [6].

Similar to LGCA, LBM performs a two-step evolution of particle distribution functions on a specific lattice model, namely particle distribution "collisions" on lattice nodes and stream "propagations" from one node to all neighbors along the lattice directions. After streaming, new local properties on lattice nodes are obtained by distribution components from neighbors, so that macroscopic properties of fluid flows can be calculated by solving this velocity discrete Boltzmann equation. In LBE, the complex collision terms of the Boltzmann equation can be replaced by a simplified relaxation model, namely the well-known Bhatnagar-Gross-Krook (BGK) model [7]. By the Chapman-Enskog expansion, this lattice BGK model can be recovered to the Navier-Stokes equations for hydrodynamics or to energy equation for heat transfer.

Simulating turbulent flows by the LBM is an attractive topic [8], [9]. The common methods for simulating turbulence are direct numerical simulation (DNS), Reynolds average numerical simulation (RANS), and large-eddy simulation (LES) [10]. The main idea of the LES is to decompose the turbulence into two parts of different scales, namely a large scale part solved by the Navier-Stokes equations and a small scale part described by a sub-grid scale (SGS) model. The LES has been used to solve many turbulent problems, e.g. simple hydraulic channels [10], gas turbine combustor flow [11], buoyant jets [12], free surface [13], and heat transfer for turbulent flows [14]. The SGS model used in this study is based on the well-known Smagorinsky model including vortex-viscous and vortex-diffusive forms [15]. Hou et al. [16] used LBM coupled with the standard Smagorinsky model to simulate two-dimensional driven cavity flow at Re up to 100,000. By solving the vorticity-stream function equations with the LES and Smagorinsky model, Chen [17] presented a lattice Boltzmann algorithm to simulate turbulent driven cavity flow. The numerical stability of this model is better than the traditional LBM, which solves mass density, pressure, and velocity for Navier-Stokes equations and has constraints of low Mach number and relaxation time. Guan et al. [18] introduced the dynamics SGS model and the dynamical system SGS model for the LBM to solve three dimensional high Re turbulent driven cavity flows. Results were compared with those obtained by the Smagorinsky model.

This paper adopts the hydrodynamic and thermal LBM algorithms to study the transport phenomena of the wavy channel, which is often employed to enhance the heat transfer efficiency in industrial processes [19]. Wang and Chen [20] used a simple coordinate transformation for the complex wavy boundary and solve the stream function, vorticity and energy equations of the fluid flow by the spline alternating-direction implicit method. The effects of the wavy geometry, Reynolds number (Re), and Prandtl number (Pr) on the skin-friction and

H. Y. Lai and S. C. Chang are with the Department of Mechanical Engineering, National Cheng Kung University, Tainan 701, Taiwan (e-mail: hylai@mail.ncku.edu.tw, mr_scchang@yahoo.com.tw).

W. L. Chen is a master's degree graduated student of the Department of Mechanical Engineering, National Cheng Kung University, Tainan 701, Taiwan (e-mail: cool-walin@hotmail.com).

This study acknowledges the support provided to this research by the National Science Council of Republic of China under Grant No. NSC 100-2221-E-006 -242 –MY3 and NSC 101-2811-E-006 -16.

Nusselt number (Nu) were discussed. By the finite element method, Alawadhi [21] studied the steady fluid flow and heat transfer in a wavy channel of 25< Re<1000 with a linearly increasing waviness at the entrance region.

Since turbulent flows are common in nature and engineering, the present study focuses on the turbulent transport phenomena of fluid flow in wavy channels. The LES method is adopted for the LBM simulation of turbulence. As a benchmark, the laminar and turbulent backward-facing step flows are simulated first to validate the feasibility of this LBM-LES method for an open flow system. The result of the reattachment length is compared with other experimental and simulation data [22]–[25]. For wavy channels, the effects of wavy geometry, Reynolds number and Prandtl number on hydrodynamic and heat transfer phenomena are discussed simultaneously. The magnitude of drag and heat transfer efficiency are evaluated by inspecting the skin-friction coefficient ($\mathrm{Re}\,C_f$) and the Nusselt number on the wavy surface.

II. Numerical Methods

A. Lattice Boltzmann Hydrodynamic Model

In the LBM simulation of incompressible flows, the continuity equation and Navier-Stokes equations are solved by calculating the evolution of density distribution function according to the LBE on the lattice model. The Boltzmann equation with the BGK model can be written as follows:

$$\frac{\partial f}{\partial t}+\vec{v}\cdot\frac{\partial f}{\partial \vec{x}}=\frac{1}{\tau_f}\left(f^{eq}-f\right) \tag{1}$$

where $\vec{v}$ is microscopic velocity, and τ_f is the relaxation time for the density distribution function, f, towards the local equilibrium. The equilibrium distribution function f^{eq} is related to the Maxwell-Boltzmann equilibrium distribution. By applying a lattice model of a discrete velocity set, (1) is transformed into the discrete LBGK form and discretized in the time and space domain as

$$\begin{aligned} &f_\alpha\left(\vec{x}+\vec{e}_\alpha\Delta t,t+\Delta t\right)-f_\alpha\left(\vec{x},t\right)\\ &\quad=-\frac{1}{\tau_f}\left[f_\alpha\left(\vec{x},t\right)-f_\alpha^{eq}\left(\vec{x},t\right)\right] \end{aligned} \tag{2}$$

where $f_\alpha\left(\vec{x},t\right)$ and $\vec{e}_\alpha$ are the component of density distribution function and lattice velocity vector in α direction of the lattice model. Equation (2) represents that in each time step, the stream and collision steps are performed individually at nodes with different lattice directions Therefore, this algorithm is suitable for parallel computation.

In the LBM simulation, the common lattice model is the DnQb model [26], which refers to the number n of dimensional sublattices and to the discrete number b of spatial translation lattice vectors. This present work adopts the D2Q9 lattice model [6] for both the hydrodynamic and thermal analysis of flows. The discrete velocity set of D2Q9 model in Fig. 1 is defined as

$$\begin{cases} \vec{e}_0=(0,0)\\ \vec{e}_{1,3},\vec{e}_{2,4}=(\pm c,0),(0,\pm c)\\ \vec{e}_{5,6,7,8}=(\pm c,\pm c) \end{cases} \tag{3}$$

where $c=\Delta x/\Delta t=\Delta y/\Delta t$ is the lattice streaming speed related to the run time step, Δt, and the grid spacing Δx and Δy. The density equilibrium distribution function is given by

$$f_\alpha^{eq}=\rho\omega_\alpha\left[1+\frac{\vec{e}_\alpha\cdot\vec{u}}{c_s^2}+\frac{\left(\vec{e}_\alpha\cdot\vec{u}\right)^2}{2c_s^4}-\frac{u^2}{2c_s^2}\right] \tag{4}$$

where $\vec{u}\left(\vec{x},t\right)$ is the velocity vector at the lattice node of position $\vec{x}$. The weight parameters are $\omega_0=4/9$, $\omega_{1,2,3,4}=1/9$, and $\omega_{5,6,7,8}=1/36$ respectively. The local density and velocity are obtained by

$$\rho=\sum_\alpha f_\alpha \tag{5}$$

$$\vec{u}=\frac{1}{\rho}\sum_\alpha f_\alpha\vec{e}_\alpha \tag{6}$$

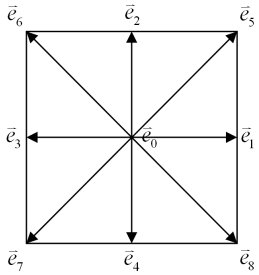

Fig. 1 D2Q9 model for LBM simulation

By the Chapman-Enskog expansion, this LBGK model can be recovered to the governing equations of incompressible flow at low Mach number with the pressure, $p=\rho {c_s}^2$, related to the lattice sound speed, $c_s=c/\sqrt{3}$. The kinematic viscosity is given by $\nu=c_s^2\left(\tau_f-0.5\right)\Delta t$.

B. Lattice Boltzmann Thermal Model

Similar to the hydrodynamic model, the macroscopic energy equation can be derived from a LBM algorithm for the temperature distribution function by Chapman-Enskog expansion. The thermal LBM model used in this paper is proposed by Shan [27], which is based on the model for simulating flows with multi-phases and -components [28]. In this model, the heat transfer of fluid flow is calculated by the evolution equation of temperature distribution function, $g_\alpha\left(\vec{x},t\right)$, as

$$g_\alpha\left(\vec{x}+\vec{e}_\alpha\Delta t, t+\Delta t\right)-g_\alpha\left(\vec{x},t\right) = -\frac{1}{\tau_g}\left[g_\alpha\left(\vec{x},t\right)-g_\alpha^{eq}\left(\vec{x},t\right)\right] \quad (7)$$

where τ_g is the relaxation time. The temperature equilibrium distribution function for the D2Q9 lattice model is given by

$$g_\alpha^{eq} = T\omega_\alpha\left[1+\frac{\vec{e}_\alpha\cdot\vec{u}}{c_s^2}+\frac{\left(\vec{e}_\alpha\cdot\vec{u}\right)^2}{2c_s^4}-\frac{u^2}{2c_s^2}\right] \quad (8)$$

The local macroscopic temperature is calculated as

$$T=\sum_\alpha g_\alpha \quad (9)$$

The diffusivity is $\kappa = c_s^{\,2}\left(\tau_g-0.5\right)\Delta t$.

C. LBM-LES Method

In the large-eddy simulation, the physical quantity Φ is decomposed into large and small scale parts by the filtering process as follows [10]

$$\bar{\Phi}=\frac{1}{\Delta^3}\cdot\int_{-\Delta/2}^{\Delta/2}\int_{-\Delta/2}^{\Delta/2}\int_{-\Delta/2}^{\Delta/2}\Phi(\bar{\xi},t)G(\bar{x}-\bar{\xi})d\xi_1 d\xi_2 d\xi_3 \quad (10)$$

where Φ is the large scale physical quantity after filter process, and Δ is the filter length equal to the mesh length. The spatial filter function, G, is the box filter function as follows,

$$G\left(\bar{x}-\bar{\xi}\right)=\begin{cases}1 & ,\left|\bar{x}-\bar{\xi}\right|\le 0.5\Delta\\ 0 & ,\left|\bar{x}-\bar{\xi}\right|>0.5\Delta\end{cases} \quad (11)$$

By filtering the density and temperature distribution function, the hydrodynamic and thermal LBM-LES models with the same forms as before filtering can be obtained [16].

In the LBM-LES model, the viscosity are replaced by the equivalent quantity, $\nu_{total}=\nu+\nu_t$. By applying the Smagorinsky model, the eddy viscosity, ν_t, is represented as

$$\nu_t=\left(C_s\Delta\right)^2\left|\bar{S}\right| \quad (12)$$

where C_s is the Smagorinsky constant of a positive value. In this paper, the Smagorinsky constant is fixed as $C_s=0.1$. The magnitude of strain rate tensor $\left|\bar{S}\right|$ is calculated by

$$\left|\bar{S}\right|=\frac{\sqrt{\tau_f^2+\dfrac{18\sqrt{2}\left(C_s\Delta\right)^2 Q^{\frac{1}{2}}}{\rho}}-\tau_f}{6\left(C_s\Delta\right)^2} \quad (13)$$

where Q represents the magnitude of the non-equilibrium stress tensor, Π_{ij}, and is calculated as

$$Q=\Pi_{ij}\Pi_{ij} \quad (14)$$

$$\Pi_{ij}=\sum_\alpha e_{\alpha i}e_{\alpha j}\left(f_\alpha-f_\alpha^{eq}\right) \quad (15)$$

Similarly, the equivalent diffusivity, $\kappa_{total}=\kappa+\kappa_t$, is used for the thermal LBM-LES model with introducing the eddy diffusivity, κ_t. For a fluid flow of specific Reynolds number, $\mathrm{Re}=UL/\nu$, and Prandtl Number, $\mathrm{Pr}=\nu/\kappa$, ν and κ can be calculated according to the characteristic velocity and length of the flow field. The eddy diffusivity is also obtained by defining the sub-grid Prandtl Number as $\mathrm{Pr}_t=\nu_t/\kappa_t$.

D. Boundary Conditions and Convergence Criteria

In the LBM simulation, the boundary conditions are implemented by calculating the unknown components of distribution function on boundary nodes after streaming process. These unknowns are due to no propagation from the boundary into the flow and can be solved by applying appropriate method. In this study, the no-slip boundary condition of the stationary wall is realized by the unknown-index algorithm [6] and the common bounce-back rule [29]. The boundary condition of a given velocity or temperature is implemented by the forced-equilibrium method [16] as

$$f_\alpha\left(\vec{x}_b,t+\Delta t\right)=f_\alpha^{eq}\left(\vec{x}_b,t\right) \quad (16)$$

$$g_\alpha\left(\vec{x}_b,t+\Delta t\right)=g_\alpha^{eq}\left(\vec{x}_b,t\right) \quad (17)$$

where $\vec{x}_b$ represents the position at the boundary node.

For laminar flows, the criteria of convergence are as follows,

$$\frac{\sum_{i,j}\left|\vec{V}\left(\vec{x}_{i,j},t+\Delta t\right)-\vec{V}\left(\vec{x}_{i,j},t\right)\right|}{\sum_{i,j}\left|\vec{V}\left(\vec{x}_{i,j},t\right)\right|}\le 1.0\times10^{-7} \quad (18)$$

$$\frac{\sum_{i,j}\left|T\left(\vec{x}_{i,j},t+\Delta t\right)-T\left(\vec{x}_{i,j},t\right)\right|}{\sum_{i,j}\left|T\left(\vec{x}_{i,j},t\right)\right|}\le 1.0\times10^{-7} \quad (19)$$

In the turbulence, the unsteady flow phenomena are captured by evaluating the time average of physical quantities.

III. Results and Discussion

In the LBM-LES simulation, all equations and physical quantity are non-dimensionalized by the lattice length, lattice speed, and reference density, ρ_0. The dimensionless temperature is defined as $T^*=(T-T_{in})/(T_w-T_{in})$. The numerical simulation is confirmed to be grid independent.

A. Benchmark

Fig. 2 is the schematic view of the backward-facing step flow. The expansion ratio and the Reynolds number are defined as $ER = H/h = 2$ and $\mathrm{Re} = U_{in}H/\nu$ with the average velocity of the fully-developed inlet flow, $U_{in} = 0.1c$. This inlet flow with a constant temperature at $T = T_{in}$ is placed at a distance of $40h$ from the step. At the outlet of $L_{out} = 100h$, the flow with a fixed reference pressure is assumed to be fully developed, i.e. $\partial U/\partial x = \partial V/\partial x = \partial T/\partial x = 0$. All stationary walls adopt no-slip boundary conditions and a high constant temperature $T = T_w > T_{in}$. The Prandtl number and subgrid Prandtl Number are fixed to 1.0 and 0.7.

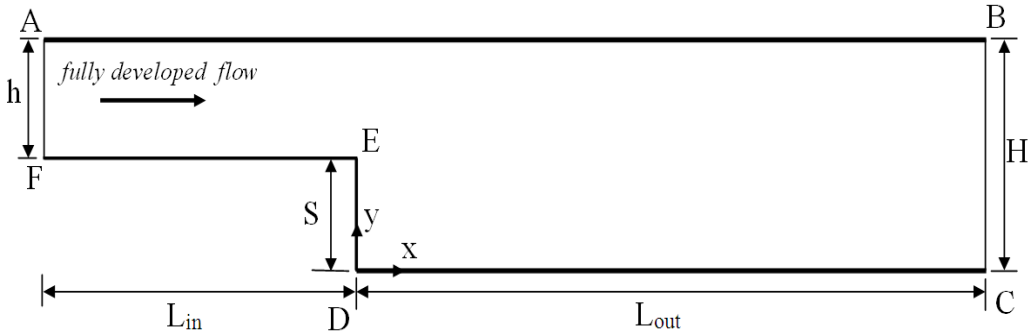

Fig. 2 Schematic view of the backward-facing step flow

In the backward-facing step flow, the separation and reattachment phenomena produce the recirculation region downstream the step. As Re increases, the main recirculation region downstream the step is enlarged accompanying with a secondary recirculation region produced near the upper wall. Fig. 3 shows the reattachment length of main recirculation region in laminar flows. The present results are close to other numerical and experiment results [22]–[24]. In turbulent backward-facing step flows, more small transient vortices behind the step are formed. The secondary vortex near upper wall is also smaller than that of laminar flow. Armaly et al. [22] indicated the main reattachment length almost kept constant at Re≧ 6,600. The results by LBM-LES model is listed in Table I with comparison to Armaly et al. [22] and Jongebloed's work [25].

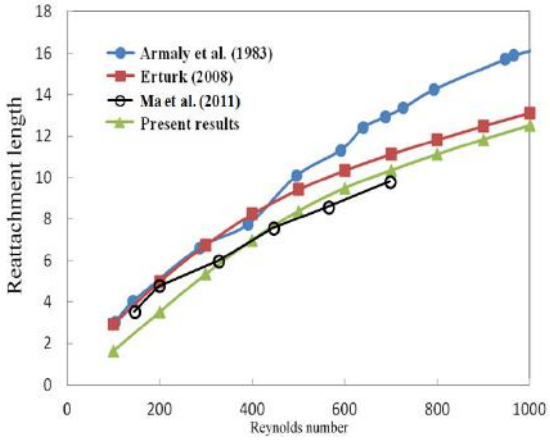

Fig. 3 Reattachment points of laminar backward-facing step flow at different Re

TABLE I
REATTACHMENT LENGTHS FOR TURBULENT BACKWARD-FACING STEP FLOWS

Re	Armaly *et al.* [22]	Jongebloed [25]	Present results
6600	8.05909	-	8.84
7000	8.01919	6.92	8.68
8000	8.0211	6.80	8.1
9000	-	-	7.8

In the thermal field, the cold fluid from inlet is heating by the hot walls via the heat transfer between walls and fluid, and hence the fluid temperature is increased downstream, as shown in Figs. 4 and 5 for laminar and turbulent flows respectively. In laminar cases, an intermediate region of cold fluid is formed and expanded as Re increases. The thermal diffusivity is dominant near the wall boundary and in the region of recirculation. In turbulent cases, the flow field is strongly perturbed, and therefore the convective effect is dominant everywhere including wall boundaries and recirculation regions. The temperature distribution of fluid downstream is uniform with no intermediate region found, i.e. the fluid heating, or namely the wall cooling, is very fast and efficient in turbulence.

B. Transport Phenomena in Wavy Channel Flows

Fig. 6 shows the schematic view of the wavy channel flow in this study. The shape of the upper wavy-wall profile is given as

$$S(x) = L + a\sin\left[\pi(x - L_{in})/L\right] \tag{20}$$

The amplitude-wavelength ratio α is defined as $\alpha = a/L$, and the Reynolds number is defined as $\mathrm{Re} = U_{in}L/\nu$. As in the backward-facing step flows, the cold fluid of $T = T_{in}$ flows through hot wavy surfaces of $T = T_w > T_{in}$ and turns into a fully developed flow at the outlet with a fixed reference pressure. The flat walls are also given a high temperature at T_w in turbulent

cases, but considered to be adiabatic in laminar cases for comparison with Wang and Chen's results [20]. In addition, all flat and wavy boundaries are no-slip.

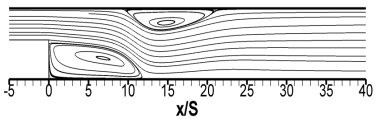

(a)

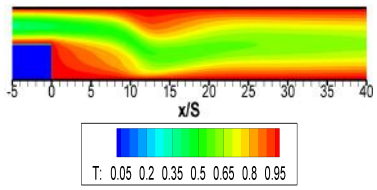

(b)

Fig. 4 (a) Streamlines and (b) temperature distribution of backward-facing step flows at Re=900

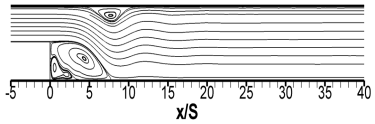

(a)

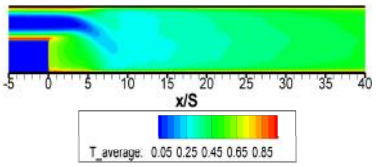

(b)

Fig. 5 (a) Streamlines and (b) temperature distribution of turbulent backward-facing step flows at Re=9000

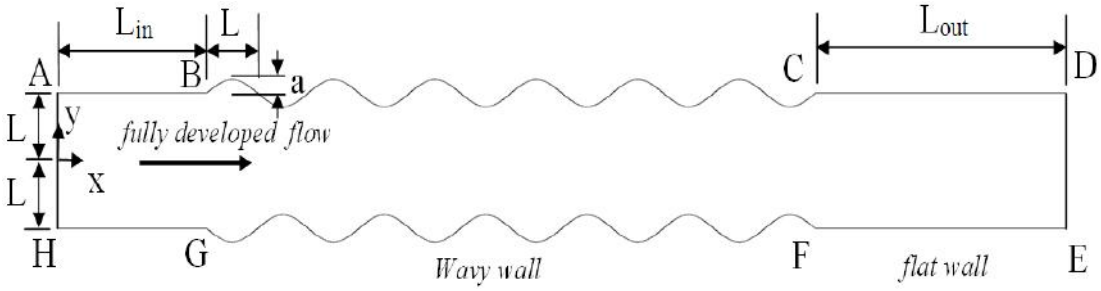

Fig. 6 Schematic view of the wavy channel flow

To estimate the heat transfer effect and the magnitude of drag in the wavy channel flow, the Nusselt number (Nu) and the skin-friction coefficient ($\mathrm{Re}\,C_f$) on the lower wavy boundary (G-F) are calculated. The local Nusselt number is defined as

$$Nu_x = h_x H / K_f = -\left(\frac{\partial T}{\partial n}\right) L / (T_w - T_{in}) \tag{21}$$

where h_x and K_f are heat transfer coefficient and thermal conductivity respectively. The temperature gradient with respect to the orientation normal to the surface is calculated by

$$\frac{\partial T}{\partial n} = \sqrt{\left(\frac{\partial T}{\partial x}\right)^2 + \left(\frac{\partial T}{\partial y}\right)^2} \tag{22}$$

The skin-friction coefficient is defined as $C_f = \tau_w / (\rho U_{in}^2)$. The shear stress on the surface given by

$$\tau_w = \mu\left(\frac{\partial u}{\partial y} + \frac{\partial v}{\partial x}\right)_{y=S(x)} \tag{23}$$

Yields

$$\mathrm{Re}\,C_f = \frac{H}{U_{in}}\left(\frac{\partial u}{\partial y} + \frac{\partial v}{\partial x}\right)_{y=S(x)} \tag{24}$$

Fig. 7 is the distribution of skin-friction coefficients and Nusselt number in the laminar wavy channel flow of Pr= 6.93 at Re=500. The results present the same tendency with the results by Wang and Chen [20] except for the skin-friction coefficients at wave troughs in the cases of $\alpha = 0.2$. As fluid flowing into the wave troughs, the flow phenomena are restrained in the recirculation regions with low velocities. These would weaken the heat convection effects and give a negative skin-friction coefficient. On the contrary, fluids in the sections of wave crests are accelerated because of the narrowed passages in a symmetric wavy channel. Therefore, drag forces upwind the wave slopes are intensified and increase the skin-friction coefficients on the wave crests. These phenomena also contribute to the convective heat transfer effect of the wavy surface and give peaks of the Nusselt number on the crests. As shown in Fig. 7, the maximum skin-friction coefficient and Nusselt number occur on the first wave crest, which is the entrance of the wavy sections in the channel, and then decay

downstream. The case of $\alpha = 0$ represents the fluid flowing through a smooth channel in which the skin-friction coefficient and Nusselt number are decreased fast. Naturally, larger amplitude causes a greater influence on not only drag forces but also heat convection effects. In the case of $\alpha = 0.2$, a small vortex is formed behind the last wavy surface and also causes negative skin-friction coefficients.

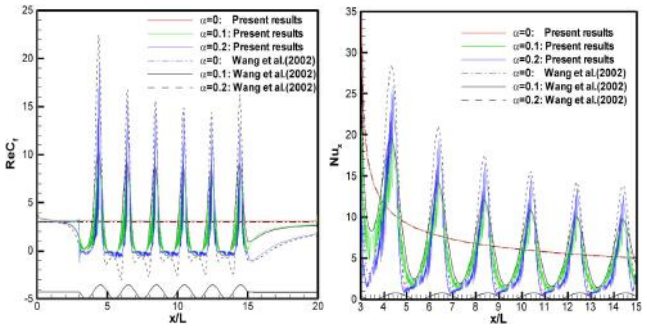

(a) (b)

Fig. 7 Distribution of (a) the skin-friction coefficients and (b) Nusselt number in the laminar wavy channel flow of Pr=6.93 at Re=500

In the simulation of turbulence, the Prandtl number is fiexd as Pr=1 with a subgrid Prandtl Number of 0.7. The average streamlines and isotherms of the turbulent wavy channel flow at Re=5000 are shown in Figs. 8 and 9. In the case of $\alpha = 0.1$, the structures of transient vortices at wavy troughs are the same as in laminar cases, and hence the tendency of skin-friction coefficient and Nusselt number are similar to those in the laminar cases except for the magnitude, as shown in Fig. 10. In turbulence, the heat convection effects are enhanced greatly by the fast and perturbed flow phenomena as well as the magnitude of drag force on the wavy surface. Although the Prandtl number in the turbulent cases is smaller than in laminar cases, the convection effects give larger and no-decayed Nusselt number on every wave crest, as sown in Fig. 10 (b).

As the amplitude increases to $\alpha = 0.2$, the vortices in the wave troughs are enlarged accompanying with small secondary ones formed near the surface. Fig. 10 indicates that these secondary vortices of the same velocity direction as flows upstream can cause the negative skin-friction coefficients at troughs changing into positive values inversely. Furthermore, the convection effects at the troughs are also improved. Fig. 11 is the distribution of skin-friction coefficient and Nusselt number for the turbulent case of $\alpha = 0.2$ at different Reynolds number. The results show the magnitude of drag and heat convection in turbulence of the wavy channel flow is reduced as Re decreases. Actually, the effects of the secondary vortices at troughs are weak in the case of Re=3000.

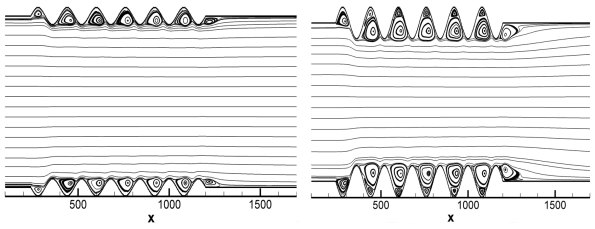

(a) (b)

Fig. 8 Turbulent streamlines of the wavy channel flow with (a) α=0.1 and (b) α=0.2 at Re=5000

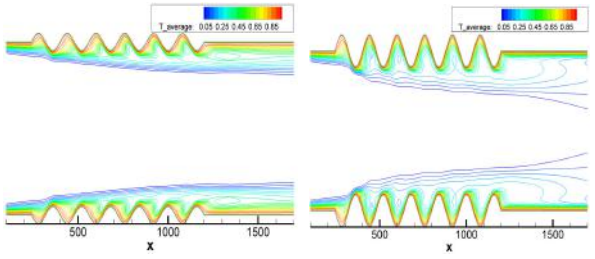

(a) (b)

Fig. 9 Turbulent isotherms of the wavy channel flow of Pr=1 with(a) α=0.1 and (b) α=0.2 at Re=5000

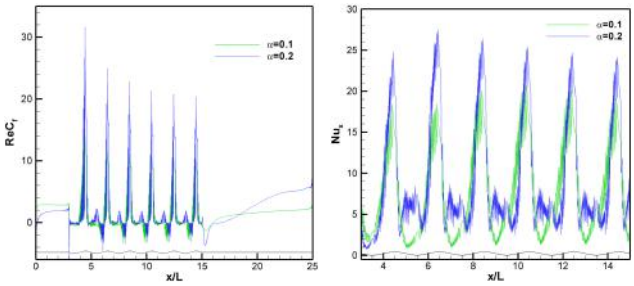

(a) (b)

Fig. 10 Distribution of (a) the skin-friction coefficients and (b) Nusselt number in the turbulent wavy channel flow of Pr=1 at Re=5000

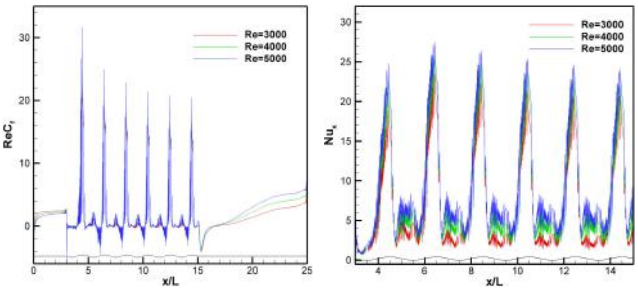

(a) (b)

Fig. 11 Distribution of (a) the skin-friction coefficients and (b) Nusselt number in the turbulent wavy channel flow of Pr=1 with α=0.2 at different Reynolds number

REFERENCES

[1] G. R. McNamara and G. Zanetti, "Use of the Boltzmann equation to simulate lattice-gas automata," Phys. Rev. Lett., vol. 61, pp. 2332–2335, 1988.

[2] J. Zhang, "Lattice Boltzmann method for microfluidics: models and applications," Microfluid. Nanofluid., vol. 10, pp. 1–28, 2011.
[3] D. Grunau, S. Chen and K. Eggert, "A lattice Boltzmann model for multiphase fluid flows," Phys. Fluids, vol. 5, pp. 2557–2562, 1993.
[4] C. K. Chen, S. C. Chang, and S. Y. Sun, "Lattice Boltzmann method simulation of channel flow with square pillars inside by the field synergy principle," CMES-Comp. Model. Eng. Sci., vol. 22, pp. 203–215, 2007.
[5] Z. Guo and T. S. Zhao, "Lattice Boltzmann model for incompressible flows through porous media," Phys. Rev. E, vol. 66, p. 036304, 2002.
[6] S. C. Chang, Y. S. Hsu, and Chen CL, "Lattice Boltzmann simulation of fluid flows with fractal geometry: An unknown-index algorithm," J. Chin. Soc. Mech. Eng., vol. 32, pp. 523–531, 2011.
[7] P. L. Bhatnagar, E. P. Gross, and M. Krook, "A model for collision processes in gases. I. Small amplitude processes in charged and neutral one-component systems," Phys. Rev., vol. 94, pp. 511–521, 1954.
[8] S. Chen and GD Doolen, "Lattice Boltzmann model for fluid flows," Annu. Rev. Fluid Mech., vol. 30, pp. 329–364, 1998.
[9] H. Chen, S. Kandasamy, S. Orszag, R. Shock, S. Succi, and V. Yakhot, "Extended Boltzmann kinetic equation for turbulent flows," Science, vol. 301, pp. 633–636, 2003.
[10] J. W. Deardoff, "The use of subgrid transport equations in a three-dimensional model of atmospheric turbulence," J. Fluids Eng.-Trans. ASME, vol. 95, pp. 429–438, 1973.
[11] W. W. Kim, S. Menon, and H. C. Mongia, "Large eddy simulation of a gas turbine combustor flow," Combust. Sci. Technol., vol. 143, pp. 25–62, 1999.
[12] X. Zhou, K. H. Luo, and J. J. R. Williams, "Study of density effects in turbulent buoyant jets using large-eddy simulation," Theor. Comput. Fluid Dyn., vol. 15, pp. 95–120, 2001.
[13] G. Yu, E. J. Avital, and J. J. R. William, "Large eddy simulation of flow past free surface piercing circular cylinders," J. Fluids Eng.-Trans. ASME, vol. 130, p. 101304, 2008.
[14] S. M. Hashemian, M. Rahnama, and M. Farhadi, "Large eddy simulation of turbulent heat transfer in a channel with a square cylinder," Heat Transf. Eng., vol. 33, pp. 1052–1062, 2012.
[15] J. S. Smagorinsky, "General circulation experiments with the primitive equations─ I. The basic experiment," Mon. Weather Rev., vol. 91, pp. 99–164, 1963.
[16] S. Hou, J. Sterling, S. Chen, and G. D. Doolen, "A lattice Boltzmann subgrid model for high Reynolds number flows," In *Pattern Formation and Lattice Gas Automata,* A. T. Lawniczak and R. Kapral, Ed. Fields Institute Communications American Mathematical Society, 1996, pp. 151–166.
[17] S. Chen, "A large-eddy-based lattice Boltzmann model for turbulent flow simulation," Appl. Math. Comput., vol. 215, pp. 591–598, 2009.
[18] H. Guan and C. Wu, "Large-eddy simulations of turbulent flows with lattice Boltzmann dynamics and dynamical system sub-grid models," Sci. China Ser. E-Technol. Sci., vol. 52, pp. 670–679, 2009.
[19] T. A. Rush, T. A. Newell, and A. M. Jacobi, "An experimental study of flow and heat transfer in sinusoidal wavy passages," Int. J. Heat Mass Transf., vol. 42, pp. 1541–1553, 1999.
[20] C. C. Wang and C. K. Chen, "Forced convection in a wavy-wall channel," Int. J. Heat Mass Transf., vol. 45, pp. 2587–2595, 2002.
[21] E. M. Alawadhi, "Forced convection flow in a wavy channel with a linearly increasing waviness at the entrance region," J. Heat Transf.-Trans. ASME, vol. 131, p. 011703, 2009.
[22] B. F. Armaly, F. Durst, J. C. F. Pereira, and B. T. Schonung, "Experimental and theoretical investigation of backward-facing step flow," J. Fluid Mech., vol. 127, pp. 473–496, 1983.
[23] E. Erturk, "Numerical solutions of 2-D steady incompressible flow over a backward-facing step. Part I: High Reynolds number solutions," Comput. Fluids, vol. 37, pp. 633–655, 2008.
[24] K. Ma, W. L. Wei, L. L. Wang, X. J. Zhao, "Large eddy numerical simulation of flows over a backward-facing step," International Symposium on Water Resource and Environmental Protection, vol. 4, pp. 3024–3026, 2011.
[25] L. Jongebloed, "Numerical study using FLUENT of the separation and reattachment points for backwards-facing step flow," Master's thesis in mechanical engineering, Rensselaer Polytechnic Institute, 2008.
[26] Y. H. Qian, D. d'Humiéres, P. Lallemand, "Lattice BGK models for Navier-Stokes equation," Europhys. Lett., vol. 17, pp. 479–484, 1992.
[27] X. Shan, "Simulation of Rayleigh-Bénard convection using a lattice Boltzmann method," Phys. Rev. E, vol. 55, pp. 2780–2788, 1997.
[28] X. Shan and H. Chen, "Lattice Boltzmann model for simulating flows with multiple phases and components," Phys. Rev. E, vol. 47, pp. 1815–1819, 1993.
[29] D. P. Ziegler, "Boundary conditions for lattice Boltzmann simulation," J. Stat. Phys., vol. 71, pp. 1171–1177, 1993.

Dr. Hsin-Yi Lai received his Ph.D. from the University of Wisconsin at Madison in 1984. He is currently working in National Cheng-Kung University as a full-time faculty member. Dr. Lai's research interests include engineering modeling of various micro-macro systems, design of experiments, and universe exploration. He had experiences in the application of modeling techniques for many different engineering systems. Dr. Lai is currently active in the professional societies of ASME, SME, ASEE and CSME.

Dr. Shing-Cheng Chang received his Ph.D. in Mechanical Engineering from National Cheng Kung University in Taiwan, 2010. He is a postdoctoral fellow of Department of Mechanical Engineering, National Cheng Kung University in Taiwan. His major research areas include computational fluid dynamics and nanotechnology. He has published 20 research papers in international journals, books, and conferences.

應用晶格波茲曼法於背向階梯紊流強制對流熱傳分析

張勳承[1]、陳朝光[1]*、陳維霖[1]
[1]國立成功大學 機械工程學系
Email: ckchen@mail.ncku.edu.tw

國科會計畫編號 NSC 100-2221-E-006-243-MY2

摘要

本文採用晶格波茲曼方法結合大渦模擬法，來模擬高雷諾數並具有熱傳效應的強制對流紊流場。晶格波茲曼方法由於數值穩定性的原因，大部分的研究都在低雷諾數的流場，而本文利用了邊界條件處理方法及大渦模擬來解決此問題，因此可以模擬高雷諾數的流場。本文模擬的問題為背向階梯流場，範圍涵蓋了層流及紊流。由於晶格波茲曼方程式為非穩態方程式，在求解紊流的時候無法得到穩態解，因此本文採用時間平均的方式得到時間平均解。本文研究的問題與已知文獻的實驗及模擬結果相比較，均非常吻合。本文也計算流場之表面摩擦係數以及紐賽數，來探討雷諾數對流場阻力大小以及對流熱傳效應的影響。

*關鍵字：*晶格波茲曼法、大渦模擬、背向階梯紊流

1. 前言

晶格波茲曼方法(Lattice Boltzmann Method，LBM)[1] 是目前熱門的數值方法之一，在許多領域上已有不錯的成果。晶格波茲曼方法是從氣體動力理論中的波茲曼方程式演化而來的，此方法在巨觀（macroscopic）的觀點上是連續的，在微觀（microscopic）的觀點上是離散的，因此被稱為介觀的方法（mesoscopic）。許多傳統計算流體力學(Computational fluid dynamics，CFD)難以解決的問題，都可以由晶格波茲曼方法來解決。

LBM 與 CFD 有許多不同的地方，LBM 是從微觀的角度出發，以稀薄氣體假設為基準，計算分子團的運動情形。分子動力學模擬(molecular dynamics simulation)的基本思想是直接考慮每個分子的運動行為，而 LBM 以考慮分子團的行為來取代各個分子的行為，因此節省了相當多的計算量。如今我們用微觀分子團的行為描述，利用統計力學，我們可以從微觀進入介觀。使用 Chapman-Enskog 展開可以將介觀的 Boltzmann 方程式推導成巨觀的 Navier-Stokes 方程組。相反地，CFD 是從巨觀方程式出發，經由離散得到離散方程式來求解。LBM 的優點有物理意義清晰、邊界條件處理簡單、程式撰寫容易、平行運算能力佳等等。本研究即利用 LBM 方法來研究背向階梯之紊流強制對流熱傳問題。

紊流廣泛的存在於自然界與工程中的流動現象，為複雜的多尺度不規則流動，因此紊流的求解十分困難。紊流的預測主要是採用物理實驗與數值模擬，在計算機快速發展下，紊流的數值模日益受到重視。

目前常用的數值模擬方法有三種，分別為直接模擬 (DNS) 、大渦模擬 (LES) 及雷諾平均模擬 (RANS)[2]。直接模擬是直接求解流動的巨觀方程式，但由於紊流是多尺度的不規則流動，因此要得到流場的所有訊息所需的計算資源非常大，因此目前只能模擬簡單的紊流場。雷諾平均模擬是工程中常用的方法，此方法將統御方程式進行時間平均後建立模型。雷諾平均模擬不需要計算各種尺度的紊流擾動量，它只計算平均運動，因此它的空間辨別率低，計算量小。大渦數值模擬主要思想是將物理量分成大尺度與小尺度的量，主要求解大尺度的物理量，而小尺度的擾動則建立亞格子模型來近似。本文採用大渦模擬並使用渦黏及渦擴散亞格子模型，利用 Smagorinsky 模式來得到渦黏及渦擴散系數。

2. 數值方法

2.1 速度場模型

本文採用D2Q9 模型[3]來模擬二維流場，令晶格傳遞速度 $c = \Delta x/\Delta t = \Delta y/\Delta t$ ，其中 Δx 和 Δy 為粒子在空間中的移動距離。晶格波茲曼法描述出定義於由位置和速度展開的相空間中之粒子分佈函數 $f(\vec{x},\vec{V},t)$ ，其中 $\vec{x}$ 和 $\vec{V}$ 為粒子的位置向量和速度向量，t為時間。密度分佈函數的演化方程式為

$$f_i(\vec{r}+\vec{e}_i\Delta t, t+\Delta t) = f_i(\vec{r},t) - \frac{1}{\tau_v}[f_i(\vec{r},t) - f_i^{eq}(\vec{r},t)] \quad (1)$$

其中 τ_v 代表密度分佈函數趨近於局部平衡態 f_i^{eq} 的弛豫時間(relaxation time)。平衡態密度分佈函數為

$$f_0^{eq}(\vec{r},t) = \frac{4\rho}{9}\left[1 - \frac{3\vec{u}^2}{2c^2}\right],$$

$$f_i^{eq}(\vec{r},t) = \frac{\rho}{9}\left[1 + \frac{3(\vec{e}_i\cdot\vec{u})}{c^2} + \frac{9(\vec{e}_i\cdot\vec{u})^2}{2c^4} - \frac{3\vec{u}^2}{2c^2}\right], \quad i = 1,2,3,4$$

$$f_i^{eq}(\vec{r},t) = \frac{\rho}{36}\left[1 + \frac{3(\vec{e}_i\cdot\vec{u})}{c^2} + \frac{9(\vec{e}_i\cdot\vec{u})^2}{2c^4} - \frac{3\vec{u}^2}{2c^2}\right], \quad i = 5,6,7,8$$

(2)

巨觀的密度場和速度場可表示為 $\rho = \sum_i f_i$ 與 $\rho\vec{u} = \sum_i \vec{e}_i f_i$。利用Chapman-Enskog expansion以及多尺度分析[3]，在低馬赫(Mach number)數假設下可還原出不可壓縮之連續方程式以及Navier-Stokes方程式，其中 $p = c_s^2\rho$ 為壓力，$c_s = c/\sqrt{3}$ 為聲速，且運動黏滯係數為 $\nu = (\tau_\nu - 0.5)c_s^2\Delta t$。

2.2 溫度場模型

Shan 與 Chen [4]提出一個用以模擬多組分流體的多組分 LBM 模型，在該模型中假設各組分之間的互相作用足夠小，並可以忽略，因此可以大幅簡化擴散方程式。在此我們假設一個多組分流動系統中存在 S 種組分，且各種組分間的相互作用小到可以忽略，我們可以用 n_α^σ 代表第 σ 種組分的分布函數，而 Boltzmann 方程式的演化方程如下

$$n_\alpha^\sigma(\vec{x}+\vec{e}_\alpha\Delta t, t+\Delta t) - n_\alpha^\sigma(\vec{x},t) = -\frac{1}{\tau_\sigma}\left[n_\alpha^\sigma(\vec{x},t) - n_\alpha^{\sigma,eq}(\vec{x},t)\right], \quad (3)$$

其中 $\sigma = 1,....,S$。若不考慮不同組分間的相互作用，則可以假設所有的分布函數使用相同的速度 $\vec{u}'$ 如下

$$\vec{u}' = \sum_{\sigma=1}^{S}\frac{m_\sigma n_\sigma \vec{u}_\sigma}{\tau_\sigma} \Big/ \sum_{\sigma=1}^{S}\frac{m_\sigma n_\sigma}{\tau_\sigma}, \quad (4)$$

其中 m_σ 與 n_σ 分別為第 σ 種組分的分子質量與數密度，且第 σ 種組分的密度及動量分別為 $\rho_\sigma = m_\sigma n_\sigma$ 與 $\rho_\sigma\vec{u}_\sigma = m_\sigma n_\sigma \vec{u}_\sigma$。

此模型也可以應用到含有溫度變化的流場中，若黏滯熱耗散與可壓縮功可忽略，則溫度可以看成是一個隨著流體運動的被動標量，且滿足擴散方程式。因此我們可以使用兩個組分來模擬含有溫度變化的流場。其中組分 1 用來模擬速度場，組分 2 用來模擬溫度場。D2Q9 模型的平衡態分布函數如下:

$$n_\alpha^{\sigma,eq} = n_\sigma\omega_\alpha\left[1 + \frac{\vec{e}_\alpha\cdot\vec{u}}{c_s^2} + \frac{(\vec{e}_\alpha\cdot\vec{u})^2}{2c_s^4} - \frac{u^2}{2c_s^2}\right] \quad (5)$$

$\sigma = 2$ 為

$$g_\alpha^{eq} = T\omega_\alpha\left[1 + \frac{\vec{e}_\alpha\cdot\vec{u}}{c_s^2} + \frac{(\vec{e}_\alpha\cdot\vec{u})^2}{2c_s^4} - \frac{u^2}{2c_s^2}\right] \quad (6)$$

溫度演化方程為

$$g_\alpha(\vec{x}+\vec{e}_\alpha\Delta t, t+\Delta t) - g_\alpha(\vec{x},t) = -\frac{1}{\tau_g}\left[g_\alpha(\vec{x},t) - g_\alpha^{eq}(\vec{x},t)\right] \quad (7)$$

$$\sum_\alpha g_\alpha = T \quad (8)$$

利用 Chapman-Enskog 展開可得到模型對應的巨觀溫度方程式

$$\frac{\partial T}{\partial t} + \frac{\partial(u_j T)}{\partial x_j} = \kappa\frac{\partial^2 T}{\partial x_j\partial x_j} \quad (9)$$

其中 $\kappa = (\tau_g - 0.5)c_s^{\,2}\Delta t$ 為熱擴散系數。

2.3 LBM結合大渦模擬法

在大渦模擬中，將紊流的物理量或稱擾動量分成大尺度與小尺度兩種型式，下面將以大渦跟小渦分別代表大尺度與小尺度的擾動。大尺度的渦幾乎包含所有的紊流動能，且與流動的邊界形狀有很大的關係，是高度各相異性的，大部分的質量及動量運輸都由大渦來完成。而小尺度的渦主要是耗散紊流動能，小渦與邊界形狀幾乎沒有關係，因此可近似為各性同性的。根據此觀念，大渦的運動由 Navier-Stokes 方程組來描述，小渦的運動則由建立模型來近似，藉此增大空間及時間步長，減少計算量。大渦模擬利用過濾函數過濾掉紊流中小尺度的擾動，過濾完的物理量即為大尺度的物理量，而小尺度的擾動用亞格子模型來近似，最常用的是渦黏及渦擴散形式的 Smagorinsky 模式[2]。

對 LBM 模型進行過濾後，並引進渦黏滯系數 ν_t，即有效運動黏滯系數為

$$\nu_{total} = \nu_0 + \nu_t \quad (10)$$

其中 ν_0 為分子黏滯系數。使用 Smagorinsky 模式可得

$$\nu_t = (C_s\Delta)^2\left|\overline{S}\right| \quad (11)$$

$$\left|\overline{S}\right| = \sqrt{2\overline{S_{ij}}\,\overline{S_{ij}}} \quad (12)$$

式中 Δ 為網格長度，C_s 為 Smagorinsky 常數，在一般情況之下，C_s 為 0.1~0.2，本研究中設定為 0.1。$\left|\overline{S}\right|$ 為剪應變率張量的大小，可由下式求得，

$$\left|\overline{S}\right| = \frac{\sqrt{\tau_{f\_0}^{\,2} + \frac{18\sqrt{2}(C_s\Delta)^2 Q^{\frac{1}{2}}}{\rho}} - \tau_{f\_0}}{6(C_s\Delta)^2}。 \quad (13)$$

其中

$$Q = \Pi_{ij}\Pi_{ij}, \quad (14)$$

$$\Pi_{ij}=\sum_{\alpha}e_{\alpha i}e_{\alpha j}\left(\overline{f_\alpha}-\overline{f_\alpha^{eq}}\right), \tag{15}$$

為非平衡態應力項。求得ν_{total}後，即可利用 2-1 節之關係式，可得流場有效鬆弛時間τ_{f_total}。

在溫度場模型方面，令$\Pr=\nu_0/\kappa_0$為分子的 Prandtl Number，$\Pr_t=\nu_t/\kappa_t$為亞格子的 Prandtl Number，其中κ、κ_t分別為分子熱擴散系數與渦熱擴散系數，即有效熱擴散系數

$$\kappa_{total}=\kappa_0+\kappa_t \tag{16}$$

由於熱擴散系數可藉由 Prandtl Number 與黏滯系數求得，因此只要先求出黏滯系數便能得到熱擴散系數。再透過 2-2 節之關係式，可得溫度場有效鬆弛時間τ_{g_total}。在分子 Prandtl Number 約為 1 的流體中，亞格子 Prandtl Number 約為 0.7。在大多數的工程應用上這個模型是可行的。

由上述推導可知，在晶格 Boltzmann 方法中引入大渦模擬只需要修改在演化方程式中的鬆弛時間即可辦到，且不影響平衡態分布函數的型式及其求解流程。此外，應變率張量的大小也可以由非平衡態分布函數的關係直接給定，與傳統 CFD 中的以有限差分法求應變張率不同，此方法在計算上更快速且操作簡單。

2.4 邊界條件設定

圖一為背向階梯流場之示意圖，無因次長度h=1，階梯擴張比ER=H/h=2，L_{in}=40，L_{out}=100。雷諾數定義為$\mathrm{Re}=2U_{in}h/\nu$，其中U_{in}為入口的平均速度。在邊界條件方面，採用Chang等人[3]、Zou與He[5]、以及Hou等人[6]所提出的方法來計算速度場與溫度場之邊界未知分布函數。入口邊界為完全展開流：

$$U(y)=-\frac{6U_{in}}{h^2}\left[y^2-(2S+h)y+\left(S^2+hS\right)\right],\quad V=0 \tag{17}$$

以及等溫邊界條件($T=T_{in}$)。出口的壓力為固定值，而速度與溫度採取全展邊界條件

$$\frac{\partial U}{\partial x}=\frac{\partial V}{\partial x}=\frac{\partial T}{\partial x}=0。 \tag{18}$$

壁面為無滑移邊界與等溫邊界條件($T=T_w>T_{in}$)。

3. 結果與討論

3.1 背向階梯層流與紊流對流熱傳分析

Armaly 等人[7]使用 ER=1.942，做了三維的背向階梯實驗以及數值模擬，結果顯示在 Re≦1200 為層流，1200<Re<6600 為過渡區，Re≧6600 為紊流。在層流區及紊流區可視為二維流動，而在過渡區有強烈的三維性，因此本文只探討層流與紊流的部分，並與 Armaly 等人[7]的結果做比較，並延伸計算溫度場，觀察局部熱傳效應。

圖二與圖三為層流的流線與溫度圖，雷諾數範圍為 400≦Re≦1000，可以看到迴流區會隨著雷諾數上升而變大，而上壁面的第二個迴流區則在 Re>400 之後出現，迴流區變大的是因為對流效應變強。圖四為層流再接觸點長度隨 Re 變化圖，再接觸點長度(x1/S)定義為流動經過階梯後，在階梯下游產生的第一個封閉的迴流區，此迴流區與下壁面接觸且速度為零的點稱為再接觸點。本文結果與 Armaly 等人[7]的實驗結果(ER=1.942)及 Erturk [8]的數值結果(ER=1.942)做比較。由圖顯示趨勢相同，在高雷諾數方面則與 Erturk [8]的結果比較接近。由溫度變化圖可以看到隨著雷諾數升高，中間低溫的區域越來越明顯，這是因為對流效應變強，熱傳導的效應相對於熱對流的效應來得弱所導致的。在階梯後方第一個迴流區與上壁面第二個迴流區的地方溫度較高，這是因為迴流區為封閉流場，不易將熱傳至下游。

使用LBM-LES模擬紊流時會出現非穩態的現象，為了捕捉紊流的流場特性，將使用時間平均值的概念來計算紊流場中的物理量。圖五分別為Re=1000及Re=6600時，在X=L_{in}+S，Y=S的位置上觀測的速度隨時間變化圖。由圖五(a)可以看到經過5萬個Δt後，流場逐漸達到穩態，速度不隨時間而改變，因此在此雷諾數下流動可確定為層流。由圖五(b)可以看到速度隨著時間不斷變動，因而無法得到穩態解，因此在可證實為紊流，其時間平均速度將趨於定值。

圖六為紊流的平均流線圖，雷諾數範圍為6600≦Re≦9000。由圖可以看到第一個迴流區裡面還包含了許多小旋渦，且再接觸點長度維持在 8 左右，且上壁面也有第二個迴流區，跟層流相比紊流的迴流區大小並沒有特別大，反而比雷諾數 1000 時來得小，且迴流區的大小在雷諾數變化那麼大的情況下並沒有很大的變化，這是比較特別的現象。表一為紊流再接觸點長度的比較表，可以看到使用 LBM-LES 模擬的結果與 Armaly 等人及 Jongebloed 的結果符合。驗證了 LBM-LES 在模擬層流及紊流的準確度。圖七為紊流的平均溫度圖，可以看到溫度圖大致上趨勢已經差不多，因為流場已趨於固定的原故，且中間的低溫區比起層流更為明顯，這是因為紊流的對流效應比層流更強。

3.2 雷諾數對表面摩擦係數與紐賽數的影響

在本文中，以階梯下游下壁面之表面摩擦係數(Skin-friction coefficient，ReCf) [10]來評估阻力大小：

$$\mathrm{Re}\,C_f=\frac{2L}{U_m}\left(S_{12}\right)_{y=S(x)} \tag{19}$$

其中 L 為特稱長度，U_m為特徵速度，S_{12}為剪應變率張量，

$$S_{12}=-\frac{3}{2}\frac{1}{\tau\rho}\Pi_{12}, \tag{20}$$

Π_{12} 可由(15)式求得。熱傳效應則由紐賽數(Nusselt number，Nu)來評估，

$$Nu_x = -\left(\frac{\partial T^*}{\partial n}\right)L, \quad (21)$$

其中 $T^* = (T - T_{in})/(T_w - T_{in})$。

圖八為層流下雷諾數對表面摩擦係數與紐賽的影響，可以看到表面摩擦係數從零開始隨著往下游移動而下降，直到第一個再接觸點附近有最小值，因為迴流區的 x 方向速度為負，且速度越靠近再接觸點時越大。表面摩擦係數在第一個再接觸點的下游開始增加，在雷諾數低的情況下(Re=400)，上壁面沒有迴流區，因此表面摩擦係數將趨於定值。在較高雷諾數時，上壁面處會產生迴流區，導致下方的流體受到壓縮，造成速度加快，因此表面摩擦係數將會繼續增加，並在接近上壁面再接觸點位置附近有最大值。在下游因為流動逐漸趨於完全發展流，因此摩擦係數將保持定值。雷諾數的升高將會導致再接觸點長度增加，因此雷諾數越高，摩擦係數的最小值及最大值位置都會往下游移動。若流體性質及特徵長度固定，雷諾數增加相當於速度變快，因此摩擦係數的變化也會更劇烈。

由圖八(b)可以看到 Nu 從零開始越往下游越大，且在下壁面的第一個迴流區及上壁面的第二個迴流區的部分 Nu 很快速的增加，這是因為流體在迴流區內對流熱傳效果較差，越接近再接觸點越好。而在迴流區下游開始變小，越下游則下降的幅度越平緩，這是因為到了下游時流體溫度與壁面溫度的差距已經變小了，形成熱完全展開流。當雷諾數越大時，會產生越大的對流效應，對流熱傳效果也因此變大，所以 Nu 會隨著雷諾數的增加而上升。

圖九為紊流下雷諾數對表面摩擦係數與 Nu 之影響，其中數值均為時間平均值。可以看到在紊流下，不同雷諾數對表面摩擦係數與 Nu 的差異並不大，這是因為在紊流下第一個再接觸點的位置幾乎保持定值，因此流場的趨勢大致相同。而紊流的摩擦係數之最小值跟層流的相比也小得多，這是因為雷諾數較高，造成摩擦係數的變化較為劇烈。而紊流的 Nu 與層流的相比，還是可以看到紊流的 Nu 最大值比層流的還大，因為雷諾數越高，對流熱傳效應也越強。

4. 結論

本研究用晶格波茲曼方法結合大渦模擬法，來模擬背向階梯之強制對流熱傳流場，範圍涵蓋層流以及高雷諾數之紊流。而本文利用了邊界條件處理方法及大渦模擬來解決 LBM 在高雷諾數模擬時的數值不穩定的問題，因此可以模擬高雷諾數的流場。由於晶格波茲曼方程式為非穩態方程式，在求解紊流的時候無法得到穩態解，因此本文採用時間平均的方式得到時間平均解。

本文分析背向階梯層流以及紊流之流場結構，並與已知文獻的實驗及數值模擬數據比較，結果均相當吻合。而在溫度場方面，可發現受速度場影響而有不同的對流熱傳效應。本研究同時計算流場之表面摩擦係數以及紐賽數，來探討雷諾數對流場阻力大小以及對流熱傳效應的影響，結果顯示雷諾數之效應對層流與紊流並不相同。

5. 誌謝

本論文為國科會編號NSC 100-2221-E-006-243-MY2之計畫，由於國科會的支持，使本計畫得以順利進行，特此致上感謝之意。

6. 參考文獻

1. D. W. Gladrow, Lattice-Gas Cellular Automata and Lattice Boltzmann Models: An Introduction, Springer, 2000.
2. 張兆順、崔桂香、許春曉，”湍流大渦數值模擬的理論和應用”，清華大學出版社，2008。
3. S. C. Chang, Y. S. Hsu, and C. L. Chen, “Lattice Boltzmann simulation of fluid flows with fractal geometry: An unknown-index algorithm”, J. CSME, Vol. 32(6), pp.523~531, 2011.
4. X. Shan and H. Chen, “Lattice Boltzmann model for simulating flows with multiple phases and components.” Phys. Rev. E, Vol. 47, pp. 1815-1819, 1993.
5. Q. Zou and X. He, “On pressure and velocity boundary conditions for the lattice Boltzmann BGK model”, Phys. Fluids, Vol. 9(6), pp.1591-1598, 1997.
6. Hou, S.,& Sterling, J.,& Chen, S., and Doolen, G. D., “A lattice Boltzmann subgrid model for high Reynolds number flows,” in Pattern Formation and Lattice Gas Automata, edited by A. T. Lawniczak and R. Kapral, Fields Institute Communications Vol. 6 (AMS, Providence), pp. 151–166, 1996.
7. B. F. Armaly, F. Durst, J.C.F. Pereira, and B. Schonung, “Experimental and theoretical investigation of backward-facing step flow”, J. Fluid. Mech., Vol. 127, pp. 473–496., 1983.
8. E. Erturk, “Numerical solutions of 2-D steady incompressible flow over a backward-facing step, Part I: High Reynolds number solutions”, Computers & Fluids, Vol. 37, pp. 633–655, 2008.
9. L. Jongebloed, “Numerical Study using FLUENT of the Separation and Reattachment Points for Backwards-Facing Step Flow”, An Engineering Project Submitted to the Graduate Faculty of Rensselaer Polytechnic Institute in Partial Fulfillment of the Requirements for the degree of Master of Engineering, 2008.
10. C. C. Wang and C. K. Chen, “Forced convection in a wavy-wall channel”, International Journal of Heat and Mass Transfer, Vol. 45, pp. 2587-2595., 2002

表一 紊流之再接觸點長度比較表

Re	Armaly [7]	Jongebloed [9]	Present results
6600	8.05909	-	8.84
7000	8.01919	6.92	8.68
8000	8.0211	6.80	8.1
9000	-	-	7.8

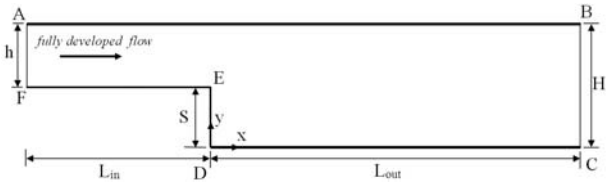

圖一 背向階梯流場之示意圖

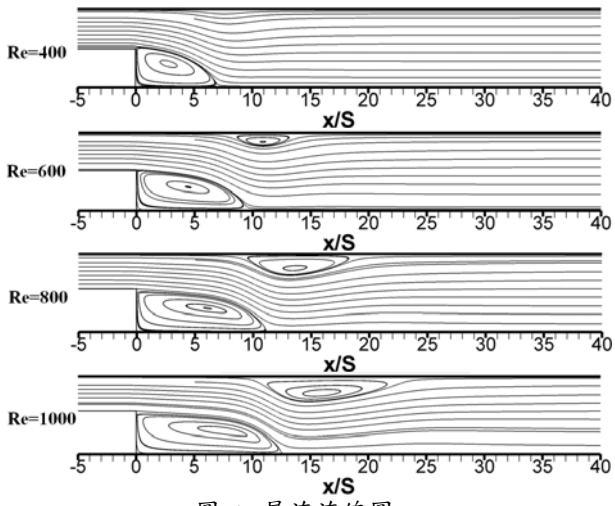

圖二 層流流線圖。

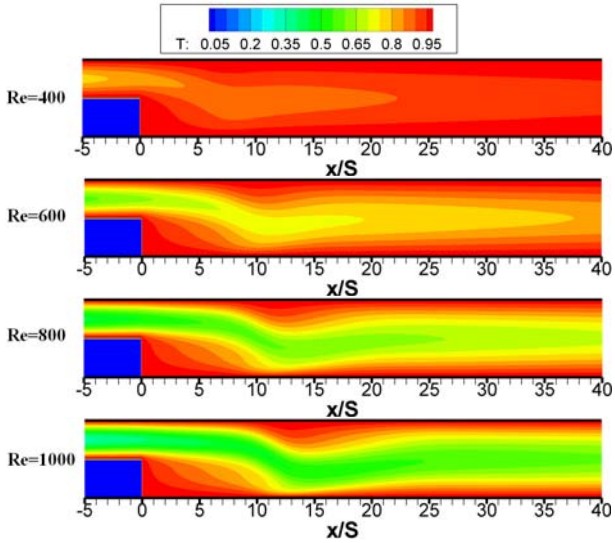

圖三 層流溫度圖。

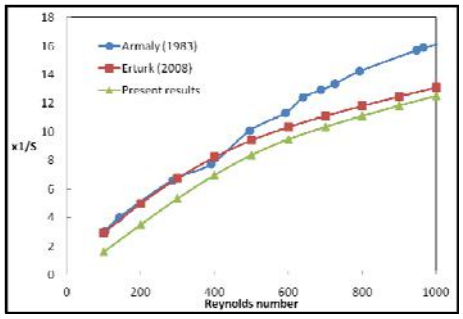

圖四 層流之再接觸點長度隨 Re 變化圖

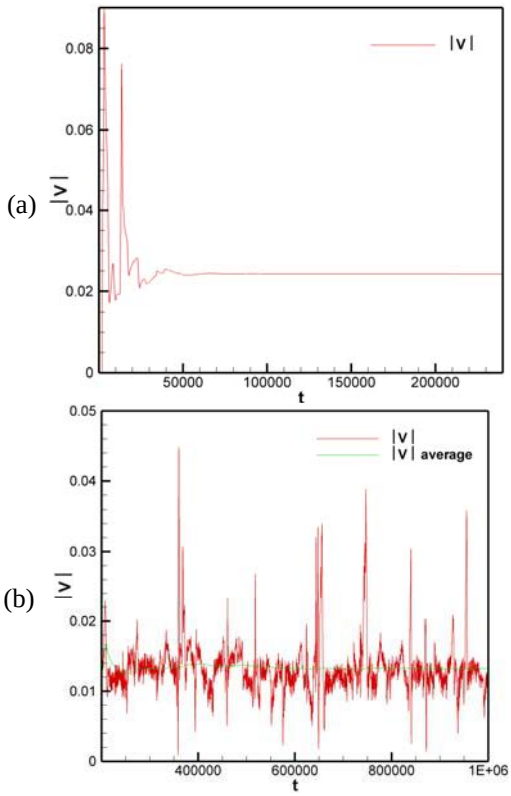

圖五 速度隨時間之變化。(a) Re=1000，層流；(b)Re=6600，紊流。

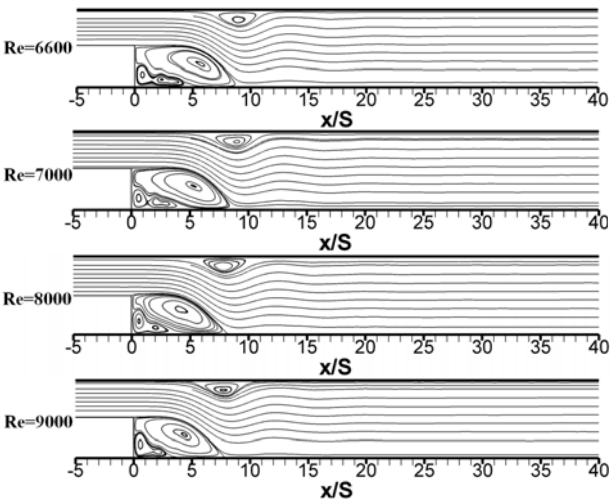

圖六 紊流平均流線圖。

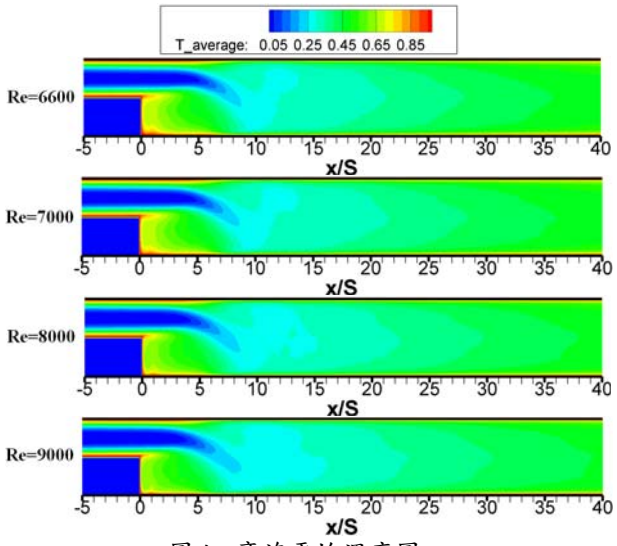

圖七　紊流平均溫度圖。

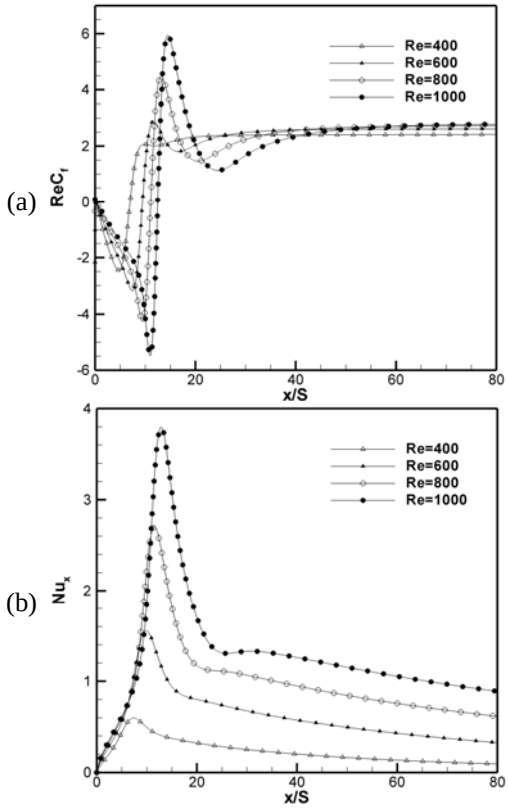

圖八　雷諾數對背向階梯層流之(a)表面摩擦係數與(b)紐賽數之影響比較圖

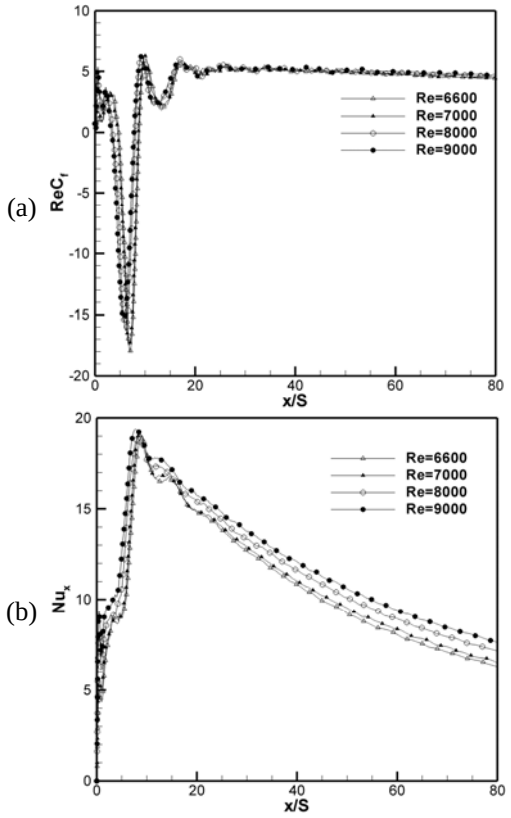

圖九　雷諾數對背向階梯紊流之(a)平均表面摩擦係數與(b)平均紐賽數之影響比較圖

Lattice Boltzmann Method of Turbulent Convective Heat Transfer of Backward-Facing Step Flow

S. C. Chang [1], C. K. Chen [1]* and W. L. Chen[1]
[1]Department of Mechanical Engineering,
National Cheng-Kung University
Email: ckchen@mail.ncku.edu.tw

NSC Project No. NSC 100-2221-E-006-243-MY2

Abstract

In this study, the large eddy simulation is introduced into the lattice Boltzmann method, and applied to numerically solving turbulent flows with convective heat transfer of backward facing step flow. This flow fields are considered as two-dimensional incompressible flow, include laminar and turbulent flows. Because lattice Boltzmann equation is an unsteady equation, the steady solution can't be obtained in the simulation of turbulent flows. Therefore, the time average solutions are calculated the numerical simulations. The results are compared with other experimental and numerical results, and obtained good consistency.

Keywords: lattice Boltzmann method, large eddy simulation, backward-facing step turbulence